DOE/ET-53088-391 IFSR #391

Resonances and Transport in the Sawtooth Map

*Q. Chen, I. Dana**, *J.D. Meiss, N.W. Murray*†, and *I.C. Percival*‡
Institute for Fusion Studies
The University of Texas at Austin
Austin, Texas 78712

August 1989

* *Department of Nuclear Physics, Weizmann Institute of Science, Rehobot 76011, ISRAEL*
† *Mail Code 130-33, California Institute of Technology, Pasadena, CA 91125*
‡ *School of Mathematical Sciences, Queen Mary College, University of London, Mile End Road, London E1 4NS, U.K.*

Resonances and Transport in the Sawtooth Map

Q. Chen*, I. Dana†J. D. Meiss‡, N. W. Murray§, and I. C. Percival¶

August 8, 1989

Abstract

We study transport in a completely chaotic Hamiltonian system, the sawtooth map. Analytical expressions are obtained for its cantori and resonances. We show that resonances give a complete partition of phase space whenever the map is hyperbolic. The flux leaking out of a resonance is given by its turnstiles, whose form and areas are obtained analytically. When the total flux out of a resonance becomes one third the area of an island, the topology of the turnstiles changes. At the same parameter value, a horseshoe is formed corresponding to the orbits trapped within the resonance. Based on this, a coding scheme for the trapped orbits is introduced and expressions for trapped ordered orbits are obtained. The partial flux transferred from one resonance to another is determined by the degree of overlap of their turnstiles. We calculate the survival probability within a resonance using the Markov model; the results are compared with results obtained numerically and from periodic-orbit theory.

*Institute for Fusion Studies, University of Texas, Austin, TX 78712, Present address: Laboratory for Plasma Research, University of Maryland, College Park, MD 20742

†Department of Nuclear Physics, Weizmann Institute of Science, Rehovot 76100, Israel

‡Institute for Fusion Studies, University of Texas, Austin, TX 78712, Present address: Department of Applied Mathematics, University of Colorado, Boulder, CO 80309

§Mail code 130-33, California Institute of Technology, Pasadena, CA 91125

¶School of Mathematical Sciences, Queen Mary College, University of London, Mile End Road, London E1 4NS, U.K.

Contents

1 Introduction

Chaotic motion for Hamiltonian systems occurs when invariant tori have been destroyed, and results in transport of phase points from one part of the phase space to another. Estimates of the rates of this transport are required for many applications in plasma, fluid and chemical systems [1]; however, their computation by iteration of a sample of initial conditions requires a great deal of computer time and becomes prohibitive when accurate results are needed, or a large range of parameters must be scanned.

A much more efficient prescription for transport calculations can be obtained for systems with two degrees of freedom, or, equivalently, area-preserving maps. In this case transport is controlled by partial barriers [2, 3], formed from cantori and partial separatrices [4, 5]. Flux across these barriers occurs through turnstiles.

A transport model is obtained by choosing a set of partial barriers to partition phase space into regions which are connected by turnstiles. If the motion in these regions is completely "random", the transition probabilities from one to another are Markov [2, 6, 7]. While the rates obtained from this model depend on the detailed structure of the partial barriers and their turnstiles, its simplicity permits rapid computation when compared to direct iteration. However, the statistical assumptions made in the Markov model require verification; this is the problem to which we address this paper.

The phase space of a typical area-preserving map is divided between regular and irregular motions. Motion in an irregular component is strongly influenced by its boundaries, which are invariant circles. When an orbit nears such a boundary it invariably stays nearby for long periods, which implies that the motion often appears to be nearly ordered [8]. These long time correlations complicate the study of such mixed systems. Statistical approximations often omit such structures, and thus fail dramatically in predicting the long time behavior.

In this paper we use the sawtooth map [9, 10, 11], a completely chaotic system, as a test case for the Markov model. It has several advantages:

1. Cantori, partial barriers, turnstiles and resonance boundaries can all be obtained analytically.

2. These structures are completely analogous to those of piecewise linear maps [12] and even smooth maps like the standard map [2, 4]. When the nonlinear kick is large the agreement can even be quantitative. Thus the sawtooth map can be viewed as giving the behavior of a smooth system in the limit of strong chaos.

3. Other methods for calculation of some of the transport properties are available for purposes of comparison [13].

4. For all positive values of the parameter, the sawtooth map is purely chaotic. Thus, there are no invariant tori, nor boundaries to the irregular components.

In Section 2 we summarize the properties of the sawtooth map, including its symbolic dynamics, minimax periodic orbits, partial barriers and turnstiles.

In Section 3 we show that the entire phase space is partitioned into resonances, and how the definition of turnstiles has to be generalized when the Lyapunov exponent is large. Turnstile overlaps, which are essential for the Markov transport model, are explicitly calculated.

In Section 4 we obtain the properties of periodic orbits within resonances, characterize and derive them from the linear code, and provide numerical illustrations. For sufficiently large values of the parameter, we find that the set of orbits trapped within a resonance is a full horseshoe, topologically conjugate to a Bernoulli shift.

In Section 5 we review the construction of a Markov transport model. Specializing to the case of escape from a single resonance, we calculate the survival probability. When the horseshoe exists, the escape rate obtained using the Markov assumption is exact. For smaller values of the parameter, the rates are compared to one based on the entropy as well as to direct numerical iteration.

2 Partial Barriers and Turnstiles

In this section we introduce the sawtooth map [9, 10, 11] and present some new results on its dynamics. We obtain explicit formulas for the minimax ordered orbits and exhibit the geometry of the partial barriers and turnstiles of cantori.

2.1 The Sawtooth Map

A sawtooth map describes a kicked rotor subject to an impulse periodic in time and linear in the rotation angle, except for a single discontinuity. The map is area preserving on a cylinder, and is given by the equations

$$T: \begin{cases} p_{t+1} = p_t + Kf(x_t), \\ x_{t+1} = x_t + p_{t+1}, \pmod 1 \end{cases} \tag{1}$$

where $2\pi x$ is the configuration angle, so that x_t is assumed to be in the unit interval

$$0<x_t<1, \tag{2}$$

p is the conjugate momentum,

$$f(x) = x - 1/2 \qquad (0<x<1),$$

and K is a positive parameter which represents the kick strength. The impulse function $f(x)$ is discontinuous on the line $x = 0$.

Alternatively, by removing the "mod 1" from the configuration component of (1), the map can be extended to the plane. Let X_t denote the configuration on the real line. The corresponding Newtonian or Lagrangian equation of motion is then

$$\delta^2 X_t \equiv X_{t+1} - 2X_t + X_{t-1} = Kf(X_t), \tag{3}$$

where the function $f(x)$ is continued periodically outside the unit interval.

To return the configuration to the unit interval, define the sequence of integers $\{b_t\}$ [10] by

$$\delta^2 X_t = \delta^2 x_t + b_t. \tag{4}$$

Subtracting this from the right-hand side of (3) gives

$$(\delta^2 - K)x_t = -(b_t + K/2). \tag{5}$$

The advantage of this technique is that (5) is now linear, and so can be easily inverted to obtain x_t,

$$x_t = \frac{1}{2} + \sum_{s=-\infty}^{\infty} \frac{\lambda^{-|t-s|}}{\sqrt{D}} b_s, \tag{6}$$

where λ is the greater eigenvalue of the linearization of the map,

$$\begin{aligned} \lambda &= 1 + \frac{K + \sqrt{D}}{2}, \\ D &\equiv K^2 + 4K. \end{aligned} \tag{7}$$

The integers b_t are determined by the dynamics of the orbit through (5), and conversely they also determine the orbit through the inverse (Green) function (6). Because (5) and (6) are linear equations, the sequence $\{b_t\}$ is said to be a *linear code.* For a given K not all sequences $\{b_t\}$ are allowed, but only those for which the inequalities (2) are satisfied for all t. We refer to those orbits which do not satisfy (2) as *ghost* orbits [11]. As the parameter K increases a ghost orbit eventually will become a real orbit when its points all arrive in the unit interval.

2.2 Ordered Periodic Orbits

Solutions of (3) satisfying the order-preserving property

$$X_t + j < X_{t'} \Longleftrightarrow X_{t+1} + j < X_{t'+1}, \tag{8}$$

for all integers j, t, t' are known as ordered orbits. If, moreover, there exist two integers m and n such that $X_{t+n} = X_t + m$ for all t, the corresponding orbit is called *periodic.* If m and n are the smallest such integers, n is called the *period* of the orbit, and one can easily show, using (8), that m and n must be relatively prime. The *winding number* or *frequency* of the orbit is then defined by

$$\nu = m/n. \tag{9}$$

Among all periodic orbits of winding number m/n, the configuration for the ordered orbit has the absolute minimum action sum [14]:

$$W = \sum_{t=1}^{n} [\frac{1}{2}(X_{t+1} - X_t)^2 + V(X_t)], \tag{10}$$

where

$$V(x) = \frac{1}{2}K(x - \frac{1}{2})^2 \qquad (0 \leq x < 1),$$

and is continued periodically beyond this interval. The ordered periodic orbit is symmetric about the discontinuity line, where $V(x)$ assumes its maximum value. Thus, if the points of the orbit in the interval (0, 1) are labeled, in order of increasing x, by $x(l)$, $l = 0, 1, ..., n-1$, one has $x(l) = 1 - x(n - l - 1)$. If x_t is the solution of (5) with (2), we choose the origin of time so that $x_0 = x(0)$. Then, using (8) and (9), one finds that

$$x_t = x(mt), \tag{11}$$

where mt and, in general, all the arguments of the functions x_t and $x(l)$ from now on, are taken modulo n. Equation (11) can be inverted to give

$$x(l) = x_{lr}, \tag{12}$$

where r is a solution of the Diophantine equation

$$mr = 1 \pmod{n}. \tag{13}$$

Throughout this paper we use x_t to denote time ordering and $x(l)$ to denote configuration ordering.

Neighboring points on an ordered orbit define a *gap*; because of the ordering condition (8), the iterate of a gap is also a gap. If a point $x_t = x(l)$ is the right endpoint of a gap then (12) implies that $x_{t-r} = x(l-1)$ is its left endpoint. Thus we define the gap width as

$$\xi_t = x_t - x_{t-r} + \delta_{t,0}, \tag{14}$$

where $\delta_{t,0}$ is the Kronecker delta symbol with t taken modulo n. It is included in (14) to measure the gap width for points which straddle the discontinuity line.

When $K = 0$ all the gaps have equal width, so $\xi_t = 1/n$. Using the equation of motion (5), the second difference operator applied to (14) gives

$$0 = \delta^2 \xi_t = \delta^2 \delta_{t,0} + (b_{t-r} - b_t) \qquad (K = 0). \tag{15}$$

Since the points on an ordered orbit can never cross as K is varied, (15) defines the linear code for an ordered orbit for any value of K,

$$b_t = b_{t-r} + \delta^2 \delta_{t,0}. \tag{16}$$

Combining (16) with (14) and (5) for arbitrary K gives a linear second difference equation for ξ_t,

$$(\delta^2 - K)\xi_t = -K\delta_{t,0}, \tag{17}$$

which together with periodicity, $\xi_{t+n} = \xi_t$, implies

$$\xi_t = \frac{K(\lambda^{n-t} + \lambda^t)}{\sqrt{D}(\lambda^n - 1)}, \tag{18}$$

where λ and D are given by (7).

The gap at $t = 0$ is the biggest one, so we refer to it as the *principal* gap. Since the principal gap is positioned symmetrically around the discontinuity line, the first point on the orbit is

$$x(0) = x_0 = \frac{\xi_0}{2} = \frac{1}{2}\frac{K(\lambda^n + 1)}{\sqrt{D}(\lambda^n - 1)}. \tag{19}$$

The other points are obtained by adding gaps to (19), using (12),

$$x(l) = x_{lr} = x(0) + \sum_{s=1}^{l} \xi_{sr}. \tag{20}$$

A closed form for this sum is usually difficult to obtain.

In general, as the frequency of a minimizing orbit approaches an irrational number ($n \to \infty$), the orbit approaches the cantorus with that frequency [15]. On the other hand, if the frequency limits to m/n from below (or above), then the orbit approaches a minimizing orbit homoclinic to the minimizing periodic orbit with frequency m/n. We refer to this orbit using the symbol m/n_- (or m/n_+). Expressions for all these orbits are obtained directly from (18) and (20); for example, the gap function in this limit is

$$\xi_t = \frac{K}{\sqrt{D}}\lambda^{-|t|}. \tag{21}$$

This function does not depend on ν, thus every cantorus, and every minimizing homoclinic orbit have the same gaps: it is only the ordering of the gaps which depends on the frequency. In more general mappings the gap widths themselves depend explicitly on the frequency.

The ordered periodic orbit defined by (18)-(20) is the ordinary hyperbolic one, which minimizes the action sum (10). For maps (1) with continuous $f(x)$ the Poincaré-Birkhoff fixed point theorem guarantees the existence of a second ordered periodic orbit with the same winding number. This orbit is elliptic or hyperbolic with reflection, and its action sum (10) is a minimax or saddle point.

For the sawtooth map, the discontinuity disallows the use of the theorem; nevertheless, we can find a second periodic orbit, provided we adopt the convention that

$$f(x=0)=0. \tag{22}$$

Applying the minimum principle subject to the constraint that one point of the orbit lies on the discontinuity line then yields a second orbit.

Let $\bar{x}_t$, $t=0,1,...,n-1$ be the points of the minimax orbit, with $\bar{x}_0=0$ and the remaining points in (0, 1). Using (22) and (5), the equation for the minimax points is

$$(\delta^2-K)\bar{x}_t=-b_t+\frac{K}{2}(\delta_{t,0}-1). \tag{23}$$

Since the orbit is ordered, (11) and (12) are satisfied if x is everywhere replaced by $\bar{x}$. Similarly the gap width of the minimax orbit is $\bar{\xi}_t=\bar{x}_t-\bar{x}_{t-r}+\delta_{t,0}$, and it has the same symbol sequence as the minimizing orbit. Combining this with (23) gives

$$(\delta^2-K)\bar{\xi}_t=-\frac{1}{2}K(\delta_{t,0}+\delta_{t-r,0}). \tag{24}$$

Comparing (24) with (17), we immediately obtain

$$\bar{\xi}_t=\frac{\xi_t+\xi_{t-r}}{2}. \tag{25}$$

Equation (25) shows that the width of every gap of the new ordered orbit is the arithmetic mean of the widths of two neighboring gaps of the corresponding hyperbolic orbit. In other words, every point $\bar{x}_t$ is the center of the interval $(x_{t-r},\ x_t)$ for $t\neq 0$. Furthermore, it is obvious that $\bar{x}_0$ is the center of the principal gap since $x_0=0$. Using this in the equation for the momentum (1), it is then easy to show that the momenta $\bar{p}_t$ are also in the centers of the gaps in the momenta p_t of the minimizing orbit. Thus, each point of the "minimax orbit" is the center of the straight-line segment joining two neighboring points of the minimizing orbit in phase space. This is illustrated schematically in Fig. 1.

In the limit $n\to\infty$, the minimax orbit becomes a minimax homoclinic orbit. If the frequency approaches an irrational number, the orbit is homoclinic to the cantorus since each of its points fall in the center of a gap of the cantorus. If the frequency limits to m/n from below (or above), then the orbit approaches the minimax orbit homoclinic to the minimizing periodic orbit with frequency m/n.

2.3 Partial Barriers and Turnstiles

An absolute barrier to transport is a curve across which there is no motion, i. e., an invariant circle. A *partial barrier*, on the other hand, is a continuous curve homotopic to the circle $p = 0$ (i. e., a rotational circle) which connects every point on a minimizing-minimax pair of orbits with a given winding number [2]. In general, such rotational circles are not absolute barriers: orbits can cross from below to above (an exception is the case $K = 0$, for which every rotational circle $p = p_0$ is an absolute barrier). The winding number of the orbits used to make the partial barrier can be rational or irrational. For the rational case, the orbits can be periodic, or can be the upper or lower homoclinic orbits to a minimizing orbit. For the irrational case the orbits correspond to a cantorus and its minimax homoclinic orbit. Unlike an invariant circle, each of these make imperfect barriers to transport.

The partial barrier can be chosen to be invariant under the action of the map with the exception of one gap, which we choose to be the principal gap. The partial barrier and its pre-image enclose a region known as a turnstile. The turnstile is divided into two parts whose areas measure the upward and downward flux through the partial barrier. These fluxes must be equal because the net flux through any rotational circle is zero [2].

The construction of partial barriers can be well illustrated by the sawtooth map. Let

$$\mathbf{G}_t = (\xi_t,\ \eta_t)$$

be the gaps of a minimizing orbit in phase space, so that ξ_t is the configuration gap and η_t is the momentum gap. These are of three types, the principal gap $\mathbf{G}_0$, the forward gaps, $\mathbf{G}_t$ with $t>0$, and the backward gaps, $\mathbf{G}_t$ with $t<0$, where

$$\mathbf{G}_t = T^t\mathbf{G}_0.$$

To begin the construction of the partial barrier, connect the endpoints of the principal gap, $\mathbf{G}_0$, with a straight-line segment (recall that this segment goes through a minimax point). The segments joining the backward gaps are the pre-images of this straight line. Similarly connect the endpoints of $\mathbf{G}_1$ with a straight-line segment; the segments for the forward gaps are the images of this segment. All these images and pre-images must be straight lines because they do not intersect the discontinuity line, and apart from this line the sawtooth map acts linearly. The collection of these straight-line segments forms a continuous, but not differentiable, rotational circle which is the partial barrier for the given orbit.

When the orbit period is infinite, this construction gives a partial barrier constructed from pieces of stable and unstable manifolds [2, 4]. For the sawtooth mapping the directions of these manifolds in phase space are constant and are parallel to the stable ($\mathbf{E}_s$) and unstable ($\mathbf{E}_u$) eigenvectors, which are [10]

$$\begin{aligned} \mathbf{E}_s &= (1,\ 1-\lambda), \\ \mathbf{E}_u &= (1,\ 1-\lambda^{-1}), \end{aligned} \tag{26}$$

where λ is given by (7). Since as t approaches infinity, the gap size converges to zero, both forward and backward segments $\mathbf{G}_t$ converge to zero length. Thus the forward gaps must be parallel to $\mathbf{E}_s$ and the backward gaps, as well as $\mathbf{G}_0$, to $\mathbf{E}_u$.

It follows from (26) that the configuration and momentum gaps are related by

$$\begin{aligned} \eta_t &= \xi_t(1-\lambda), \quad t>0, \\ \eta_t &= \xi_t(1-\lambda^{-1}), \quad t \leq 0. \end{aligned} \tag{27}$$

It is instructive to check that the sum over t of the momentum-gap widths (27), which corresponds to the net change in momentum through the cantorus, vanishes, while the gap widths (21) in the x direction sum to unity. The latter result implies that the points of the cantorus occupy zero measure. Actually, (21) implies that the cantorus has zero fractal dimension, in conformity with a more general result [16].

A turnstile is formed by the partial barrier and its pre-image in the principal gap (see Fig. 2). For the partial barrier, the two neighboring points of this gap are connected by the original straight segment in $\mathbf{G}_0$ (solid line in Fig. 2), which is parallel to $\mathbf{E}_u$ for the infinite period case. The pre-image of $\mathbf{G}_1$ gives the dashed line in Fig. 2. This line consists of three parts: two segments parallel to $\mathbf{E}_s$, and one segment on the discontinuity line. This structure forms the two triangles in Fig. 2, which define the turnstile. The lower (upper) triangle is the region of phase space which, in one iteration of the map, crosses from below (above) to above (below) the partial barrier. The equal areas of these two regions define the one-way flux $\mathcal{F}$ across the partial barrier. Using (27) and (26), this flux is

$$\mathcal{F}(\nu) = \frac{1}{2}\frac{\xi_0}{2}\frac{\xi_0}{2}(1-\lambda^{-1}+\lambda-1) = \frac{K^2}{8\sqrt{D}}. \tag{28}$$

Again the sawtooth map is special because the flux (28) does not depend on the winding number ν of the cantorus or homoclinic orbit. According to the general theory [2], the flux is given by

$$\mathcal{F}(\nu) = \Delta W = W_h - W_c, \tag{29}$$

where $W_h - W_c$ is the long time limit of the difference in actions between the minimax orbit and the corresponding minimizing orbit. One can show that (29) is valid for the sawtooth map by a straightforward but tedious calculation.

3 Resonances

In this section we consider resonances of the sawtooth map and show that they give a complete partition of phase space. Each has an upper and a lower turnstile, giving the total flux exchanged with the rest of phase space. We show that when this flux becomes larger than one third of the area of one island of the resonance, the definition of the turnstiles has to be modified. Finally, we consider the overlap of turnstiles of any two resonances which gives the partial flux escaping from one resonance to the other. The onset of turnstile overlap exhibits a threshold behavior which is determined exactly.

3.1 Geometry of Resonances

A resonance is a region of phase space corresponding to a winding number m/n [4]. Associated with each minimizing $(m,\ n)$ orbit are partial barriers for the upper and lower homoclinic orbits. The $(m,\ n)$ resonance is defined as the region of phase space bounded by these two partial barriers. The partial barriers in this case are called "partial separatrices".

Each resonance consists of n closed regions, called "islands" (see Fig. 4), one for each gap of the hyperbolic periodic orbit. The principal island lies in the principal gap and the other $n-1$ islands are its pre-images: all islands have the same area.

Partial separatrices can be obtained as the limit of a sequence of periodic orbits which approach m/n from above and below. Begin with two rational numbers m_i/n_i, for $i=0,\ 1$, which are neighbors to m/n: they satisfy $m_i n - n_i m = (-1)^i$. The minimizing periodic orbits with winding numbers

$$\nu_i^{(j)} = \frac{m_i + jm}{n_i + jn}, \tag{30}$$

approach m/n from above and below as $j \to \infty$, for $i=0$ and $i=1$, respectively; in this limit, we label the winding numbers $m/n|_{\pm}$. The corresponding orbits limit to the upper and lower minimizing orbits homoclinic to the m/n minimizing periodic orbit. The homoclinic orbits consist of an infinite number of points and approach the points of the hyperbolic periodic orbit in both directions of time.

For the $(0,\ 1)$ resonance the winding numbers (30) of the approximating periodic orbits are

$$\nu_i^{(j)} = \frac{(-1)^i}{1+j}.$$

Let $(x_t^{(j)},\ p_t^{(j)})$ be points of the periodic orbits approximating the upper homoclinic orbit, whose points we denote $(x_t^+,\ p_t^+)$. For this simple case, $m=r=1$ in (13), and using Eqs. (20) and (21), we find for the homoclinic orbit

$$x_t^+ = \begin{cases} \dfrac{1}{2} - \dfrac{\lambda^{-t}}{\lambda+1}, & t \geq 0, \\ \dfrac{1}{2} + \dfrac{\lambda^{t+1}}{\lambda+1}, & t<0. \end{cases}$$

The momenta are

$$p_t^+ = \lambda^{-|t|}\frac{\lambda-1}{\lambda+1}.$$

Expressing p_t^+ as a function of x_t^+ gives

$$p_t^+ = \begin{cases} (\lambda-1)(\frac{1}{2}-x_t^+), & t \geq 0 \\ (1-\lambda^{-1})(x_t^+-\frac{1}{2}), & t<0 \end{cases}$$

so that for $t \geq 0$ the upper partial separatrix is a straight line in the direction of the stable manifold of the fixed point (1/2, 0), and for $t<0$ it is the unstable manifold of the same fixed point. The lower partial separatrix is constructed in a similar way. The symmetry of the map implies that it is obtained by inverting the upper one through the point (0, 0).

Partial separatrices for general $(m,\ n)$ resonances may be constructed by similar calculations. Consider the nth power of the map (1). The winding numbers of the periodic approximants to the homoclinic orbits are given by (30); however, relative to the map T^n, they are given by $\hat{\nu}_i^{(j)} = n\nu_i^{(j)}$. It is easy to verify that the r-values in (13), corresponding to $\hat{\nu}_i^{(j)}$, are given simply by $r = (-1)^i$ for any j. This means that the homoclinic-orbit gaps $\mathbf{G}_t$ are adjacent for adjacent values of t. In turn this implies that, in the corresponding partial separatrices, all the gaps $\mathbf{G}_t$ for $t>0$ ($t \leq 0$) lie on a straight-line segment parallel to the stable (unstable) eigenvector. Thus the $(m,\ n)$ resonance is built by extending the stable (unstable) manifold of a given fixed point of T^n until it intersects the unstable (stable) manifold of a neighboring fixed point. The general form of the principal island of a resonance is illustrated in Fig. 3. A set of resonances at $K = 0.1$ is shown in Fig. 4a. For comparison, Fig. 4b shows some resonances of the standard map.

3.2 Resonance Partition of Phase Space

It appears in Fig. 4a that the resonances of the sawtooth map tend to fill phase space. We show here that this is indeed the case by deriving exact relations for the area of a resonance [12].

The area of a resonance, $A(m,\ n)$, is n times the area of the principal island (see Fig. 3). The latter is given simply by twice the difference between the area of the triangle $\triangle BCR$ and that of $\triangle BJH$. The segments BH and BR have slope $1-\lambda^{-1}$, while segments ER and JH have slope $(1-\lambda)$. This yields

$$\begin{aligned} Area(\triangle BJH) &= \frac{1}{2}\sqrt{D}(x_H - x_B)^2, \\ Area(\triangle BCR) &= \frac{1}{2}\sqrt{D}(x_R - x_B)^2. \end{aligned} \tag{31}$$

The quantities $2(x_R - x_B)$ and $2(x_H - x_B)$ are, respectively, the widths of the principal gap of the $(m,\ n)$ hyperbolic periodic orbit (ξ_0 in (18)) and of the principal gap of the lower homoclinic orbit (ξ_0 in (21). Using this in (31), gives

$$A(m,\ n) = \frac{nK^2}{\sqrt{D}(\lambda^n + \lambda^{-n} - 2)}. \tag{32}$$

Equation (32) implies that the predominant dependence of the area of a resonance on

the parameter K is through the residue of the hyperbolic orbit

$$\begin{aligned} R_n &\equiv \frac{1}{4}\left[2 - Tr(DT^n)\right] \\ &= \frac{1}{4}(2 - \lambda^n - \lambda^{-n}) \end{aligned} \tag{33}$$

Thus $A(m,n) \propto 1/|R_n|$. This is also found to be true for the resonances of smooth maps, in the limit of large residue [4].

Another measure of the resonances is the height $h(m,\ n) = p_E - p_H$, which is a measure of the distance between the upper and the lower homoclinic orbits in the $(m,\ n)$ resonance. By a straightforward calculation we find

$$h(m,\ n) = \sqrt{D}[x_R - x_B - (x_E - x_A)] = \frac{K}{(\lambda^n - 1)}.$$

We now consider total area $A_{Tot}(\nu)$ below the winding number ν [2, 4, 17]. This is a monotone function of ν; for irrational values of ν it is the area under the invariant circle, or under the cantorus partial barrier with the given winding number. For the irrationals $A_{Tot}(\nu)$ is continuous. On the other hand, $A_{Tot}(\nu)$ has two values for each $\nu = m/n$: the areas under the upper and lower $(m,\ n)$ partial separatrices. Thus $A_{Tot}(\nu)$ has a discontinuity at m/n which is the area of the $(m,\ n)$ resonance. Fig. 5 shows the area function for the sawtooth map. The height function $h_{Tot}(\nu)$ is defined similarly to be the total height below ν.

A monotone function with a countable set of discontinuities is known as a *devil's staircase.* If the sum of all the jumps (discontinuities) of the function is equal to its total variation, the staircase is complete.

In fact, both the height function and the area function give complete staircases for the sawtooth map. To show that the height function, $h_{Tot}(\nu)$, is complete, compute the total of the jumps for frequencies in the interval [0, 1); this is the sum of $h(m,\ n)$ over all positive n and over coprime $m<n$. Since $h(m,\ n) = h(n)$ is independent of m, the sum over m yields the Euler φ-function, i.e., the number of positive integers not greater than and relatively prime to n. Thus the sum of the jumps is [18]

$$\sum_{n=1}^{\infty} \varphi(n)h(n) = K\sum_{n=1}^{\infty} \frac{\varphi(n)}{(\lambda^n - 1)} = \frac{K}{(\lambda + \lambda^{-1} - 2)} = 1. \tag{34}$$

The total height change $h_{Tot}(1|_-) - h_{Tot}(0|_-) = 1$ because the sawtooth mapping is periodic with period 1 in the momentum direction. Since (34) shows that the total of the jumps is also one, the height devil's staircase is complete.

Consider now the case of the area function. Introducing a new variable θ, defined by $\lambda = e^{\theta}$, we can rewrite (34) as

$$\sum_{n=1}^{\infty} \frac{\varphi(n)}{(e^{n\theta} - 1)} = [4\sinh^2(\theta/2)]^{-1}.$$

Taking the derivative with respect to θ, we get

$$\sum_{n=1}^{\infty} \frac{n\varphi(n)}{\sinh^2(n\theta/2)} = \frac{\cosh(\theta/2)}{\sinh^3(\theta/2)}.$$

Transforming back to λ, shows that this is exactly the completeness relation for the area staircase

$$\sum_{n=1}^{\infty} \varphi(n) A(n) = 1 \ .$$

This completeness is identical to that obtained by Aubry for the functional dependence of the ground-state atomic mean distance on the external field in the Frenkel-Kontorova model [14].

3.3 Resonance Turnstiles

The turnstiles of a resonance are associated with its principal island (the shaded regions in Fig. 3). The flux across the upper (lower) partial separatrix corresponds to the triangles $\triangle ACE$ and $\triangle AGI$ (triangles $\triangle BHJ$ and $\triangle BFD$). For the situation depicted in Fig. 3, these triangular turnstiles give the total area leaving the resonance. This is because, for an $(m,\ n)$ resonance, the image under T^n of the closed region $LGICRHJDF$ is the principal island $LERF$. Each of the fluxes above is given by (28), thus the total flux leaving the resonance is

$$\mathcal{F}(m,\ n) = \frac{K^2}{4\sqrt{D}},\ \lambda^n \leq 3. \tag{35}$$

However, the flux across the partial separatrices is the area which escapes from a resonance per iteration only when the outgoing halves of the turnstiles are completely contained within the resonance. As the flux increases, the point I in Fig. 3 will eventually lie below the point B and the point J will lie above the point A (Fig. 6). In this case, the triangular regions $\triangle AJM$ and $\triangle BIN$ are outside the resonance, and cannot be included in the outgoing flux; in one iteration these regions are mapped from above the resonance to below the resonance or vice versa. The ingoing (outgoing) flux consists of the trapezoidal regions $CEMJ$ and $DFNI$ (the trapezoidal regions $BAMH$ and $ABNG$). The lower (upper) turnstile of the resonance should be now identified as the union of the regions $DFNI$ and $BAMH$ (the regions $CEMJ$ and $ABNG$). We call these "generalized turnstiles".

The condition for generalized turnstiles is $p_A - p_I = K/2 > p_A - p_B = h(m,\ n)$, or

$$\lambda^n > 3.$$

The total ingoing or outgoing flux is the sum of the areas of the upper and the lower generalized turnstiles

$$\mathcal{F}(m,\ n) = 2[Area(\triangle AIG) - Area(\triangle BIN)].$$

But $Area(\triangle AIG)$ is the flux (28) across the partial separatrix, and

$$Area(\triangle BIN) = (p_B - p_I)^2/(2\sqrt{D}).$$

Using $p_B - p_I = p_A - p_I - h(m,\ n)$, we obtain

$$\mathcal{F}(m,\ n) = \frac{K^2}{\sqrt{D}} \frac{\lambda^n - 2}{(\lambda^n - 1)^2},\ \lambda^n \geq 3. \tag{36}$$

These fluxes can also be obtained by taking action differences between various homoclinic orbits, including the new homoclinic intersections represented by the points M and N.

3.4 Turnstile Overlap

The total flux $\mathcal{F}(m,\ n)$ escaping from a given resonance can be divided into *partial fluxes* $\mathcal{F}(m/n{\to}m'/n')$ transferred to an infinite number of neighboring resonances $(m',\ n')$. The calculation of partial fluxes is essential for the Markov transport model, as we will see in §5. The partial flux $\mathcal{F}(m/n{\to}m'/n')$ is given by the area of overlap of an outgoing half turnstile of $(m,\ n)$ with an ingoing half turnstile of $(m',\ n')$. This is illustrated schematically in Fig. 7, for the case $m/n{>}m'/n'$. Because resonances give a complete partition of phase space, the partial fluxes must sum to the total flux

$$\mathcal{F}(m,\ n) = \sum_{m'/n'} \mathcal{F}(m/n{\to}m'/n').$$

Furthermore, one has the "detailed balance" relation

$$\mathcal{F}(m/n{\to}m'/n') = \mathcal{F}(m'/n'{\to}m/n),$$

which follows from the reversibility symmetry [2] of (1) about the discontinuity line.

Since $p_I{>}p_D$ and $p_{A'}{>}p_{B'}$ there are only five distinct cases of turnstile overlap, corresponding to different geometries. For example, in the case illustrated in Fig. 7, $p_D{<}p_{B'}$, $p_{A'}{<}p_I$, and the partial flux $\mathcal{F}(m'/n'{\to}m/n)$ is the area of the trapezoid $A'B'WV$, or

$$\mathcal{F}(m'/n'{\to}m/n) = Area(\triangle A'DV) - Area(\triangle B'DW).$$

We can solve for these areas in terms of the momenta at the points A', B', D and I to obtain

1. Triangle:
$$\mathcal{F}(m'/n'{\to}m/n) = \frac{1}{2\sqrt{D}}(p_{A'} - p_D)^2, \qquad p_{B'}{<}p_D{<}p_{A'}{<}p_I.$$

2. Trapezoid 1:
$$\mathcal{F}(m'/n'{\to}m/n) = \frac{1}{2\sqrt{D}}\left[(p_{A'} - p_D)^2 - (p_{B'} - p_D)^2\right], \qquad p_D{<}p_{B'},\ p_{A'}{<}p_I.$$

3. Trapezoid 2:
$$\mathcal{F}(m'/n'{\to}m/n) = \frac{1}{2\sqrt{D}}\left[(p_{A'} - p_D)^2 - (p_{A'} - p_I)^2\right], \qquad p_{B'}{<}p_D,\ p_I{<}p_{A'},.$$

4. Pentagon:
$$\mathcal{F}(m'/n'{\to}m/n) = \frac{1}{2\sqrt{D}}\left[(p_{A'} - p_D)^2 - (p_{A'} - p_I)^2 - (p_{B'} - p_D)^2\right], \qquad p_D{<}p_{B'}{<}p_I{<}p_{A'}.$$

5. Parallelogram:
$$\mathcal{F}(m'/n'{\to}m/n) = \frac{1}{\sqrt{D}}(p_{A'} - p_{B'})(p_I - p_D), \qquad p_I{<}p_{B'}.$$

The values of the momenta above are easily determined from those of the momenta associated with points such as L and L' in Fig. 7. For example, L is the left endpoint of the principal gap of the $(m,\ n)$ hyperbolic periodic orbit, so that $p_L = p(n-1)$. Using Eqs. (1), (12), (13), and (20), we find

$$p_L = x(n-1) - x(n-m-1) = \sum_{s=n-m}^{n-1} \xi_{sr}$$

(we assume that $n>m$). For the case $m = 1$, this becomes $p_L = \xi_1$. Using the slopes of the eigenvectors (26), and the fact that $2(x_D - x_L)$ is the width of the principal gap (ξ_0 in (18)), we obtain

$$p_D = \frac{K}{\sqrt{D}} \left[\frac{\lambda^{-1} + \lambda^{-n}}{1 - \lambda^{-n}} - \frac{\lambda - 1}{2} \right], \qquad (1,\ n) \text{ Resonance.} \tag{37}$$

Other values of the momenta can be obtained by similar calculations. For example, if $m' = 1$ as well,

$$p_{A'} = \frac{K}{\sqrt{D}} \left[\frac{1 + \lambda^{1-n'}}{1 - \lambda^{-n'}} - \frac{1 - \lambda^{-1}}{2} \right], \qquad (1,\ n') \text{ Resonance.} \tag{38}$$

The flux $\mathcal{F}(m'/n' \to m/n)$ is non-zero only if the turnstiles of the $(m,\ n)$ and $(m',\ n')$ resonances overlap; this occurs when $p_{A'} = p_D$. The parameter value at which this occurs is a complicated function in general, but for the case of $(1,\ n)$ and $(1,\ n')$ resonances ($n'>n$), (37) and (38) imply

$$\frac{\lambda^{n'} - \lambda^n}{\lambda^{n+n'} - 1} = \frac{\lambda - 1}{\lambda + 1}. \tag{39}$$

Specializing to the case $n' = n + 1$, (39) implies that the threshold value, K_c, for overlap is determined by the algebraic equation

$$\lambda^{n+n'} - \lambda^n - \lambda^{n'} - 1 = 0\ . \tag{40}$$

It it easy to show that Eq. (40) holds also in the case $(m',\ n') = (0,\ 1)$ and arbitrary n. We denote the value of the parameter for which this overlap occurs as $K_c(n)$. It is straightforward to verify from (40) that $K_c(n)$ decreases with increasing n. Fig. 8 shows that it decreases very slowly in the asymptotic regime.

Numerical evidence implies that the overlap of the $(0,\ 1)$ and $(1,\ n)$ resonances occurs last in the sense that if all rationals up to level n on the Farey tree are included, then for $K \geq K_c(n)$ every resonance overlaps with its two neighbors. This has implications, as we will see in §5, for the adequacy of finite-state Markov models.

Near the overlap threshold,

$$p_{A'} - p_D \propto [K - K_c(n)].$$

Thus, for K near $K_c(n)$, the overlap area (a case 1 triangle) always increases quadratically, as $[K - K_c(n)]^2$. This is even valid as $n \to \infty$ ($K_c \to 0$). However, this scaling does not appear to have clear physical implications, in contrast to continuous mappings like the standard map. In the latter case, the turnstile area of the last invariant circle appears to dominate the transport properties near the onset of global chaos [2]. In particular, the diffusion coefficient

D scales in the same manner as the turnstile area of the golden-mean cantorus [19]. On the other hand, there are no "dominant" cantori in the sawtooth map, since the flux (28) does not depend on the winding number ν. Thus, one may expect that the scaling of D near $K = 0$ is not the same as that of the flux. In fact, using (28), we find that the flux scales as $K^{1.5}$, while D seems to scale as $K^{2.5}$ [7]. The latter scaling cannot be attributed to the partial flux exchanged between the (0, 1) and (1, n) resonances ($n \to \infty$); rather, it emerges as a collective effect of many resonances, exchanging approximately equal partial fluxes [7].

4 Periodic Orbits within Resonances

Orbits which are trapped within a resonance give rise to the "islands around islands" structure in smooth systems [20]. This structure impedes the escape of orbits from a resonance because a minimax periodic point is encircled by librational cantori. Each cantorus has a turnstile which impedes the transport of orbits. This structure is repeated hierarchically for each stable island within the resonance. It is natural to ask if such a structure exists in the purely hyperbolic sawtooth map and how it affects the escaping dynamics.

In the smooth case some of the trapped orbits can be characterized by their rotation frequency about the central elliptic point, or their rotation frequency about another trapped orbit. For the sawtooth map, it is more convenient to characterize the set of trapped orbits in terms of an extension of the linear code. This gives a complete characterization of the trapped set.

4.1 Coding Scheme

An orbit is uniquely determined by the linear code $\{b_t\}$. For a trapped orbit, however, it is convenient to use a modified code which more naturally describes its properties. The new code is constructed from two characteristics: the resonance within which the orbit is trapped, $(m,\ n)$, and an $\mathcal{L}$-$\mathcal{R}$ symbol sequence $\{a_i\}$. To construct the latter, consider the principal island of the $(m,\ n)$ resonance. The discontinuity line divides it into two halves, call them $\mathcal{L}$ and $\mathcal{R}$ for left and right, respectively (Fig. 9). A periodic orbit within the $(m,\ n)$ resonance has a period which is multiple of n, say qn; it has q points in each island. Pick a starting point x_0 in the principal island and let $a_0 = 0$ if x_0 is in $\mathcal{L}$, otherwise $a_0 = 1$; continue for the remaining q points, letting $a_i = 0$ if x_{in} is in the $\mathcal{L}$ half and so on. Therefore $\{a_i\}$ has period q. For example, the librational ordered orbit with rotation frequency 3/8 (winding number relative to T^n) has an $\mathcal{L}$-$\mathcal{R}$ symbol sequence $[1,1,0,1,0,0,1,0]$, where we use the square brackets to denote the periodicity. This symbol sequence corresponds to the usual symbol sequence for a hyperbolic horseshoe. In fact, as we will see below, this coding scheme gives a general code for any trapped orbit of the sawtooth map.

The linear code $\{b_t\}$ is easily obtained from the $\mathcal{L}$-$\mathcal{R}$ symbol sequence. To do this define a modified coding, the c-code, by setting $c_t = u$ if the iterate of X_t crosses the discontinuity line u times from left to right; if this line is crossed u times from right to left, $c_t = -u$. From (4), the linear code is related to the c-code by

$$b_t = c_t - c_{t-1}\ . \tag{41}$$

For example, starting from the leftmost point of the (1, 3) orbit, the c-code is $[0,0,1]$, and the linear code is $[-1,0,1]$.

Without loss of generality, we may restrict ourselves to the case $0 \leq m<n$, so that $|c_i| \leq 1$ for orbit $(m,\ n)$. Suppose the c-code for this orbit is $[c_0, c_1, c_2, \ldots, c_{n-1}]$, where time 0 corresponds to the leftmost point of the orbit. The c-code for a trapped orbit is then given by

$$[1 - a_0, c_1, c_2, \ldots, c_{n-2}, a_1, 1 - a_1, c_1, \ldots, c_{n-2}, a_2, \ldots, 1 - a_{q-1}, c_1, \ldots, a_0], \tag{42}$$

where we assume that $n>2$. There is no change in c-code for points of the orbit which are not in the principal island or in its pre-image. These points cross the discontinuity in the

next iteration exactly as corresponding points of the $(m,\ n)$ orbit. At times $t = in-1$ $(i>0)$, the iterate of X_t crosses the discontinuity if and only if $a_i = 1$. At times $t = in$ $(i \geq 0)$, this crossing occurs if and only if $a_i = 0$. This explains (42). Using (41), the linear code for times $(in-1, in, in+1)$ is given by $(1,-1,0)$ when $a_i = 1$, and is $(0,1,-1)$ when $a_i = 0$.

The cases $n = 1$ and $n = 2$ are special. For $(m,\ n) = (1,\ 2)$, the c-code is given by

$$[1-a_0, a_1, 1-a_1, \ldots, 1-a_{q-1}, a_0],$$

therefore the linear code at times $(2i-1, 2i)$ is $(1,-1)$ if $a_i = 1$, and $(-1,1)$ if $a_i = 0$. The c-code for $(m,\ n) = (0,\ 1)$ is

$$[a_1 - a_0, a_2 - a_1, \ldots, a_0 - a_{q-1}],$$

therefore $b_i = a_{i+1} - 2a_i + a_{i-1}$.

If the $\mathcal{L}$-$\mathcal{R}$ symbol is [1], the linear code is the same as that of $(m,\ n)$ orbit. If $\mathcal{L}$ -$\mathcal{R}$ symbol is [0], the linear code is that of $(m,\ n)$ orbit shifted to left once. These two cases therefore do not give trapped orbits, but the usual $(m,\ n)$ orbit.

Thus we see that each $\mathcal{L}$-$\mathcal{R}$ symbol sequence corresponds to a unique linear code, and hence to a unique orbit, if it exists. An orbit exists only if each configuration point x_t, given by (6), satisfies (2).

When $\lambda^n>3$, we will show that every $\mathcal{L}$-$\mathcal{R}$ code corresponds to a real trapped orbit. This criterion is exactly that for the formation of "generalized turnstiles" (§3.3). In fact, in this case we can not only characterize the periodic points but also the whole invariant set, which is an orientation preserving horseshoe.

Consider the principal island of the resonance under the map T^n (see Figs. 10). Using the boundary of the upper and lower turnstiles, we divide this island into three regions, Fig. 10a. Upon one iteration, the upper homoclinic point G is mapped to E, and the lower homoclinic point H is mapped to F; therefore, the vertical strip $\mathcal{V}_1$ is mapped to $\mathcal{H}_1$, and $\mathcal{V}_2$ to $\mathcal{H}_2$, Fig. 10b. The middle strip $\mathcal{M}$, which is the union of the generalized turnstiles, is mapped out of the island. This defines an orientation preserving horseshoe map. The invariant set is given by the non-escaping region of the principal island under repeated application of the map in both the forward and backward directions. This is a Cantor set, and is naturally hyperbolic, thus the dynamics on this invariant set is a full two shift, i. e., is topologically conjugate to a shift map in the space of bi-infinite sequences with two symbols. This justifies our choice of $\mathcal{L}$-$\mathcal{R}$ symbols to code the dynamics. For illustration, we show the periodic horseshoe orbits in Fig. 11a.

Thus, when $\lambda>3$, or $K>4/3$, every resonance has a full horseshoe, and every $\mathcal{L}$-$\mathcal{R}$ code corresponds to a true orbit. Even for smaller K there are always horseshoes in an infinite number of resonances of the sawtooth map since $\lambda^n>3$ when n is large enough for any $K>0$.

As λ^n decreases from 3, some of the trapped orbits began to disappear, and the horseshoe is replaced by a structure similar to that of a stable island in smooth maps, as is illustrated in Figs. 11b-d. In these figures we compute orbits for all $\mathcal{L}-\mathcal{R}$ symbol sequences up to period 12. Only those orbits which satisfy (2) are real orbits and are shown in the figures.

The symbol sequence technique could also be used to code orbits which are not forever trapped within a resonance. Since the resonance partition is complete, almost all orbits can be decomposed into segments trapped within a particular resonance. Once in a resonance,

the orbit must remain for some multiple of the resonance period. During each trapped segment the $\mathcal{L}$-$\mathcal{R}$ symbol sequence corresponding to the resonance can be used.

4.2 Trapped Rotational Periodic Orbits

An orbit which is trapped in a given $(m,\ n)$ resonance, and which rotates under T^n about a point on the minimax orbit with a definite frequency, is called a *class-1* orbit [20]. We denote the rotation frequency by p/q, where p and q are relatively prime integers (p should not be confused here with the momentum!). In Fig. 12 we show such an orbit as a function of the parameter. This orbit is born with all points at the minimax point at $K = 0$ (it is a *collapsing* orbit [11]); as K increases the points move outward.

For simplicity, we will assume that q is even, $q = 2\tilde{q}$, and that no point of the orbit lies on the discontinuity line. Of course, there can also be odd period ordered orbits. In fact, by symmetry, there are at least two of them with the same rotation frequency. One has an extra point on the left side of the discontinuity, and the other has one more point on the right.

For the even-period case, symmetry implies that there are precisely $\tilde{q}$ points on each side of the discontinuity in the principal island. Following Fig. 13, denote the point on the minimax orbit at $x = 0$ by O, and let $\mathbf{R}_0$ be the vector connecting the right endpoint of the principal gap, R, to the first point of the orbit. We choose this point so that it makes the smallest angle (measured in a clockwise sense around O) with the discontinuity line. The vector $\mathbf{R}_0$ can be written in the basis of the stable and unstable eigenvectors:

$$\mathbf{R}_0 = a\mathbf{s} + b\mathbf{u}, \tag{43}$$

where $\mathbf{s}$ is the vector from R to E, and $\mathbf{u}$ is the vector from R to F. Our problem is to determine the coefficients a and b.

To this end, consider repeated applications of the map T^n. Each iteration of this map generates a new point in the principal island, and after q such iterations we must arrive back at the starting point. Since the orbit is ordered with rotation frequency p/q, it stays on the same side of the discontinuity as the starting point for $t_1 = [\tilde{q}/p] + 1 - \delta_{p,1}$ iterations of T^n. Here $[x]$ denotes the integer part of x. During the first $t \le t_1$ iterations we have $\mathbf{R}_0 \to \mathbf{R}_t$, where

$$\mathbf{R}_t = a\lambda^{-nt}\mathbf{s} + b\lambda^{nt}\mathbf{u},$$

from the linearity of the map. After t_1 iterations the orbit is on the other side of the discontinuity. Since the map is not linear across the discontinuity, it is convenient to now use the point L (the left endpoint of the principal gap) as the new origin. Hence we will represent points on this side of the discontinuity by vectors $\mathbf{L}_t = \mathbf{R}_t - \overrightarrow{LR}$. Since $\overrightarrow{LR} = \mathbf{s} + \mathbf{u}$ we may write

$$\mathbf{L}_t = (a\lambda^{-nt_1} - 1)\lambda^{-n(t-t_1)}\mathbf{s} + (b\lambda^{nt_1} - 1)\lambda^{n(t-t_1)}\mathbf{u},$$

for $t_1 \le t \le t_2$, where t_2 is the time at which the orbit crosses the discontinuity for the second time. In general, the lth crossing occurs at $t_l = [l\tilde{q}/p] + 1 - \delta_{l,p}$, and the time between the lth and $(l-1)$th crossing is

$$\Delta t_l = \left[\frac{l\tilde{q}}{p}\right] - \left[\frac{(l-1)\tilde{q}}{p}\right] + \delta_{l,1} - \delta_{l,p}.$$

We denote the vectors $\mathbf{R}_t$ and $\mathbf{L}_t$ after the lth crossing by $\mathbf{R}(l)$ and $\mathbf{L}(l)$. Then

$$\begin{aligned}
\mathbf{R}(1) =& a\lambda^{-n\Delta t_1}\mathbf{s} + b\lambda^{n\Delta t_1}\mathbf{u}, \\
\mathbf{L}(1) =& (a\lambda^{-n\Delta t_1} - 1)\mathbf{s} + (b\lambda^{n\Delta t_1} - 1)\mathbf{u}, \\
\mathbf{L}(2) =& (a\lambda^{-n\Delta t_1} - 1)\lambda^{-n\Delta t_2}\mathbf{s} + (b\lambda^{n\Delta t_1} - 1)\lambda^{n\Delta t_2}\mathbf{u}, \\
\mathbf{R}(2) =& \left[(a\lambda^{-n\Delta t_1} - 1)\lambda^{-n\Delta t_2} + 1\right]\mathbf{s} + \left[(b\lambda^{n\Delta t_1} - 1)\lambda^{n\Delta t_2} + 1\right]\mathbf{u},
\end{aligned} \tag{44}$$

and so on. After p crossings we arrive at the point $\mathbf{R}(p)$, which is the symmetric image of the starting point,

$$\mathbf{R}_{t_p} + \mathbf{R}_0 = \mathbf{s} + \mathbf{u}. \tag{45}$$

Using (44) and (45), we find, for $p>2$,

$$\begin{aligned}
a =& \frac{\lambda^{n\tilde{q}}}{\lambda^{n\tilde{q}} + 1}\left(1 - \sum_{s=0}^{p-2}(-1)^s \prod_{l=0}^{s}\lambda^{n(l-p)}\right), \\
b =& \frac{1}{\lambda^{n\tilde{q}} + 1}\left(1 - \sum_{s=0}^{p-2}(-1)^s \prod_{l=0}^{s}\lambda^{n(p-l)}\right).
\end{aligned} \tag{46}$$

In the special case $p = 1$ the result is

$$a = \frac{\lambda^{n\tilde{q}}}{\lambda^{n\tilde{q}} + 1}, \quad b = \frac{1}{\lambda^{n\tilde{q}} + 1}.$$

If we use (46) in equation (43), we will find some point in phase space. This point will be an initial condition for an $(np,\ nq)$ class-1 periodic orbit only if

1. The point is inside the $(m,\ n)$ principal island, and outside the turnstile regions.

2. The actual motion is that of ordered rotation with the assumed rotational frequency p/q.

These two conditions are not always satisfied. In fact, the trapped ordered orbits do not always correspond to collapsing orbits [11] – the latter bifurcate only at integer parameter values (unperturbed twist map and cat maps). This is illustrated in Fig. 14 for the orbit with rotation frequency 3/10. For small parameter values two of the points fall outside the interval $0<x<1$, and thus the orbit is a "ghost". It appears only at some non-zero parameter value.

Another example of this is the case of class-1 homoclinic orbits. It is clearly impossible to form a class-1 resonance (a chain of q islands surrounding a minimax point) from the stable and unstable eigenvectors, because these eigenvectors have constant directions throughout the phase space. The same argument shows that long period ordered orbits approximating class-1 homoclinic orbits are also non-existent.

When λ is small the collection of trapped rotational orbits looks like the conventional island structure of a smooth map. In Fig. 15, we show all the trapped rotational orbits up to period 30 for the same value of λ as in Fig. 11d. It is clear that the orbits move on the hyperbolae corresponding to the invariant manifolds of the linearization of the map about the $(m,\ n)$ orbit.

4.3 Topological Entropy

The number of periodic points trapped in a resonance grows exponentially with the period. For a period n resonance the exponent is given by the topological entropy of T^n restricted to the principal island of the resonance. Let $N_n(q,\lambda)$ be the number of periodic points in the $(m,\ n)$ principal island with period q at Lyapunov exponent $\ln(\lambda)$. It has the universal form (see below)

$$N_n(q,\lambda) = N_1(q,\lambda^n). \tag{47}$$

The topological entropy of T^n, restricted to the principal island, is

$$ent(\lambda) = \lim_{q\to\infty} \ln[N_1(q,\lambda)]/q. \tag{48}$$

Fig. 16 shows a plot of $\ln[N_1(q,\lambda)]/ent(\lambda)$ as a function of q.

When $\lambda^n>3$, the dynamics is a full two shift; therefore, there are 2^q period q points, and the entropy is $\ln(2)$.

The fact that $N_n(q,\lambda)$ has the universal form (47) follows from the fact that the dynamics in the principal island can be described geometrically. As is clear from Figs. 10, there are basically three cases: λ smaller than 2, between 2 and 3, and larger than 3. In all these cases the principal island can be divided into three regions. The central strip $\mathcal{M}$ is the union of the turnstiles or the generalized turnstiles; therefore, in studying the invariant set, we can neglect this strip. The remaining two strips, labelled $\mathcal{V}_1$ and $\mathcal{V}_2$, are the regions which stay in the resonance upon n iterations, and do not include the points on the discontinuity line. For these strips, the map is geometrically equivalent to squeezing by a factor λ^{-n} in the stable direction and stretching by a factor λ^n in the unstable direction; the left and right $(m,\ n)$ periodic points remain fixed, respectively. As shown in Fig. 10, the detailed shape of the $\mathcal{V}_1$ and $\mathcal{V}_2$ strips depends only on λ^n; therefore, the number of periodic points under the map T^n depends only on λ^n.

5 Transport

Since the dynamics of the sawtooth map for $K>0$ is chaotic, it is natural to attempt to obtain a statistical description of this motion. The problem of transport is to determine the time scale for transition from one region of phase space to another. In this section we recall the Markov model for transport introduced in [2, 7], and show that some of its predictions are exact when K is large enough. For smaller values of K the Markov predictions are approximate, though they can give quantitatively reasonable results.

5.1 The Markov Model

A Markov description of transport requires two objects, a partition of phase space into regions, and the transition probabilities from one region to another. We will use resonances for the regions, since they give a complete and countable partition of phase space. For applications, it is also useful that resonances act as a partition of the momentum variable, thus each region corresponds physically to a state with approximately fixed energy or action.

The set of trajectories which leave a resonance upon iteration are just those which have points in its upper or lower (generalized) turnstiles. Consider an ensemble of initial conditions which is spread uniformly within the resonance; the fraction which escape after one iteration is exactly

$$P^E(m,\ n) = \frac{\mathcal{F}(m,\ n)}{A(m,\ n)/n}. \tag{49}$$

Here $A(m,\ n)/n$ is the area of a single island in the resonance (see (32)), and $\mathcal{F}(m,\ n)$ is the total flux leaving the resonance (§3.3). For $\lambda^n<3$, $\mathcal{F}(m,\ n)$ is given by (35), while for $\lambda^n \geq 3$, $\mathcal{F}(m,\ n)$ is given by (36). Evaluating (49) gives then

$$P^E(m,\ n) = \begin{cases} \frac{1}{4}(\lambda^n + \lambda^{-n} - 2) = |R_n|, & \lambda^n<3, \\ 1 - 2\lambda^{-n}, & \lambda^n>3, \end{cases} \tag{50}$$

where R_n is the residue (33). As λ increases from 1, P^E increases monotonically from zero, approaching 1 as $\lambda\to\infty$.

The probability for a transition from one resonance to another is determined by the overlap of the two turnstiles. Assuming a uniform ensemble, this probability is

$$P^E(m/n\to m'/n') = \frac{\mathcal{F}(m/n\to m'/n')}{A(m,\ n)/n}, \tag{51}$$

where $\mathcal{F}(m/n\to m'/n')$ is given by the equations in §3.4.

To complete the Markov model suppose that each resonance has a density $\rho_t(m,\ n)$ of particles at time t. If we assume that the density in each resonance is, and remains uniform, then the time evolution is given by

$$\rho_{t+1}(m,\ n) = (1 - P^E(m,\ n))\rho_t(m,\ n) + \sum_{m',n'} P^E(m'/n'\to m/n)\rho_t(m',\ n').$$

To make a finite-state model we can choose a set of resonances based on some approximation scheme, such as all resonances with periods smaller than some value n_{max}, or all

resonances up to some level on the Farey tree. Since the area of resonances decreases exponentially with the period, calculations based on such a truncation should rapidly converge with period. This model will allow for global transport only if the turnstiles of all neighboring resonances overlap [7]. In the case of the sawtooth map, this can always be achieved for $K>0$ by choosing the set properly, e. g., choosing n_{max} large enough. Given such a set, the critical for overlap is determined by the criteria derived in §3.4.

The formulas for transition probabilities are exact, but refer only to the special case of a uniform density in each resonance. Even if this is initially true, uniformity is in general destroyed upon a single iteration. However, if the mixing within a resonance is rapid, so that any non-uniformity in density is smoothed, then one would expect (49) and (51) to be approximately valid for all time. That is, by the time a typical trajectory escapes from a resonance it has effectively lost memory of its previous history and the transition probabilities will be Markovian. To estimate when this is valid, note that upon each iteration of T^n, the turnstile of a resonance is stretched along the unstable manifold by a factor of λ^n; thus, roughly speaking, the effective area of the turnstiles grows to $\mathcal{F}(m,\ n)\lambda^n$. This mixing will be complete if the effective area "covers" the principal island: $\mathcal{F}(m,\ n)\lambda^n > A(m,\ n)/n$, or, from (49),

$$P^E(m,\ n) > \lambda^{-n}. \tag{52}$$

Using (50), this implies that the Markov model should be reasonable for

$$\lambda^n>3,$$

which is by now a familiar criterion. As we will see below, this criterion exactly determines the validity of (49) for the escape from a single resonance. We expect that it will also govern the validity of the Markov model more generally.

5.2 Escape from a Resonance

The simplest transport problem is the escape from a single resonance: iterate the $(m,\ n)$ resonance t times and determine the fraction of the initial area remains in the resonance up to time t. The survival probability at time t is defined to be this fraction

$$P_t^S(m,\ n) = A_t(m,\ n)/A_0(m,\ n),$$

where $A_t(m,\ n)$ is the area remaining at time t. We expect that this probability decays exponentially, since the map is hyperbolic [21], and so define the escape rate

$$\alpha(m,\ n) = -\lim_{t\to\infty} \ln(P_t^S(m,\ n)/t. \tag{53}$$

Since escape takes place only in the principal island, we may restrict consideration to the area remaining in this island under the map T^n. Thus in (53) we set $t = nq$, and let $q\to\infty$. As discussed in §4.3, the dynamics in the principal island under T^n only depends on λ^n; therefore the escape rate for any resonance can be obtained from that for the (0, 1) resonance. Letting $\alpha(\lambda)$ be the escape rate from the (0, 1) resonance at eigenvalue λ, and $t = nq$ in (53), we get

$$\alpha(m,\ n) = \alpha(\lambda^n)/n. \tag{54}$$

The universal form (54) facilitates the numerical simulation considerably.

When $\lambda>3$, we can obtain the escape rate exactly, because the dynamics restricted to the principal island is a horseshoe map (see §4.1). From Fig. 10, one can easily verify that the survival probability at time t is

$$P_t^S = (2/\lambda)^t,$$

which gives the escape rate

$$\alpha(\lambda) = \ln(\lambda/2), \qquad \lambda>3. \tag{55}$$

In this case, the dynamics is purely mixing: under each iteration the remaining area is stretched uniformly in the unstable direction, uniformly covering the width of the resonance. Thus the escape probability per iteration is the same for all time.

On the other hand, suppose that the transport is a Markov process. The probability of escape per time step is P^E (see (49); therefore,

$$P_t^S = (1 - P^E)^t \ .$$

Using (50), this gives the rate

$$\alpha_M(\lambda) = \begin{cases} -\ln\left[1 - (\lambda + \lambda^{-1} - 2)/4\right], & \lambda<3, \\ \ln(\lambda/2) \ , & \lambda \geq 3. \end{cases} \tag{56}$$

Note that Eq. (56) is identical to (55) when $\lambda>3$. Thus, for single resonance phenomena, the Markov theory is exact for $\lambda>3$, as we expected from (52).

Equation (55) can also be interpreted in the following way. Let $\mathcal{T}$ be the trapped invariant set of the resonance. Then, the escape rate is given by the difference between the Lyapunov exponent and the metric entropy, of $\mathcal{T}$ [22]:

$$\alpha_L(\mathcal{T}) = L(\mathcal{T}) - ent(\mathcal{T}) \ . \tag{57}$$

This is generally true for hyperbolic systems. For the sawtooth resonance, the Lyapunov exponent is always $\ln(\lambda)$, and the metric entropy is equal to the topological entropy (48). Furthermore, when $\lambda>3$, the topological entropy is $\ln(2)$ (§4.3), so the escape rate is given by (55).

When $\lambda<3$, the entropy, and hence α_L, can be determined numerically by computing the growth rate of the number of periodic orbits. This number decreases with decreasing λ as the various $\mathcal{L}$-$\mathcal{R}$ coded orbits cross the discontinuity and cease to exist (see §4.1). Checking the existence of the periodic orbits involves large computations which we find prohibitive when $\lambda<1.5$.

Finally, the escape rate can be computed using a Monte Carlo experiment. We start with a large number of points (typically 10^6, chosen on an evenly spaced grid within the resonance) and iterate the map. The fraction of points remaining within the resonance at time t approximates the survival probability. Fig. 17a shows the log plot of the survival probability; it appears to decay exponentially for large t. We can verify this by defining an average escape rate at time t,

$$\beta(t) = -\ln(P_t^S)/t \ . \tag{58}$$

After a single time step, P^S is exactly given by (56) in the limit when the number of points in the Monte Carlo experiment goes to infinity, since the points are uniformly distributed. For larger t the rate undergoes some oscillations before relaxing to a fixed value (Fig. 17b). These oscillations are more prominent for small λ. Beyond the oscillation region, the survival probability decays exponentially until there are too few trapped points (around 10^3) to obtain good statistics. We derive a numerical escape rate by a least-square fit to the exponential regime.

Fig. 18 shows the escape rate as a function of λ. The smooth curve is the rate given by (56). The second curve is the Lyapunov rate (57); this is computed by finding all the trapped periodic orbits up to a period such that the relative error in the rate is 2%. We are unable to calculate the entropy for small λ because the convergence with period is extremely slow and excessive computations are needed. The numerical rates, from a fit to (58), are plotted as triangles. At moderate values of λ ($1.5<\lambda<3.0$), the numerical rates tend to fall close to α_L. However, α_M is not far off, the largest discrepancy being about 10%. We conclude that α_M is a reasonable estimate of the exact rate.

For small λ, the deviation between α_M and numerical rates is larger; in fact, the two rates approach zero with different functional forms. This is shown in Fig. 19, which plots the escape rates as a function of absolute value of the residue, $|R_1| = K/4$ (see (50)). For small K, α_M in (56) scales linearly with $|R_1|$. Fig. 19 shows that the numerical rate scales with a different exponent. The least-square fit gives an exponent of 1.4 ± 0.1. This error estimate is not reliable, due to the difficulty of fitting the numerical escape-rate data to an exponential. It appears as if the exponent for the escape rate is the same as that for the flux at small residue, which is 1.5.

6 Conclusions

The sawtooth map provides a simple model for testing the assumptions of transport theories. Though the map is completely chaotic, it has ordered orbits for every rotation frequency, as do all twist maps. These orbits form the skeletal structure for a partition or coarse graining of phase space.

Resonances are formed from ordered minimizing orbits together with their stable and unstable manifolds. The resonance boundaries are called partial separatrices. We use the resonances to partition phase space since they are countable, and since their areas decrease exponentially with period. We have analytically calculated the structure of resonances and their areas, explicitly demonstrating that they give a complete partition of phase space.

Transitions from one resonance to another take place through turnstiles, whose areas we also calculate analytically. When the turnstiles of two different resonances overlap, there is a probability of direct transition from one to the other, otherwise a transition requires entering and exiting intermediary resonances. When the turnstile of one partial separatrix of a resonance becomes large, it can overlap with that of the other partial separatrix of the same resonance. In this case there is a probability of making a direct transition from below to above the resonance (or vice-versa), corresponding to this overlap area. The actual flux exchanged with the resonance is reduced; we call it the generalized turnstile.

The Markov model for transport assumes that the mixing rate within a resonance is rapid enough to smooth any non-uniformity in density. This non-uniformity is reflected in the area remaining in the resonance; if this area is spread over a resonance island within one period, due to the exponential growth of separations, then the mixing is sufficient. For the sawtooth map this criterion is exactly the same as that for formation of the generalized turnstile: the escaping flux from a resonance is greater than one third the area of one resonance island. In this case the Markov model exactly predicts the escape rate. Furthermore, the trapped set in the resonance is a horseshoe.

Even when the mixing rate is slower, the Markov model predictions for escape do not deviate more than 10% from numerical calculations of escape rates. Alternatively, calculations of escape rates based on the trapped periodic orbits, while giving accurate values, become computationally intensive when the Lyapunov exponent is small.

We expect that the Markov model will be reasonably accurate even for smooth maps, provided that the mixing criterion is satisfied. The breakdown of this criterion is likely to occur most prominently when the minimax orbit in a resonance is elliptic, and is surrounded by invariant circles. In this case the resonance should be itself partitioned into librational resonances. Whether repeated partitioning ultimately results in a model for which the mixing criterion is valid remains to be seen.

Acknowledgements

Support for this work was obtained from U.S. Department of Energy grant DE-FG05-80ET-53088, the U.K. Science and Engineering Research Council, and a NATO grant for international collaboration. This collaboration was begun during a visit by QC and JDM to Queen Mary College, we would like to thank them for their hospitality.

References

[1] J. D. Meiss, J. R. Cary, D. F. Escande, R. S. MacKay, I. C. Percival and J. L. Tennyson, Dynamical Theory of Anomalous Particle Transport, in *"Plasma Physics and Controlled Nuclear Fusion Research 1984"* (IAEA, Vienna) **3** (1985) 441-448.

H. Aref, Stirring by Chaotic Advection, *J. Fluid Mech.* **143** (1984) 1-21.

M. J. Davis, Bottlenecks to Intramolecular Energy Transfer and the Calculation of Relaxation Rates, *J. Chem. Phys.* **83** (1985) 1016-1035.

[2] R. S. MacKay, J. D. Meiss and I. C. Percival, Transport in Hamiltonian Systems, *Physica* **13***D* (1984) 55-81.

[3] D. Bensimon and L. P. Kadanoff, Extended Chaos and Disappearance of KAM Trajectories, *Physica* **13***D* (1984) 82-89.

[4] R. S. MacKay, J. D. Meiss and I. C. Percival, Resonances in Area Preserving Maps, *Physica* **27***D* (1987) 1-20.

[5] S. R. Channon and J. L. Lebowitz, Numerical Experiments in Stochasticity and Heteroclinic Oscillation, in *Nonlinear Dynamics*, R. H. G. Helleman, ed., **357** (1980) 108-118.

[6] J. D. Hanson, J. R. Cary and J. D. Meiss, Algebraic Decay in Self-Similar Markov Chains, *J. Stat. Phys.* **39** (1985) 327-345.

J. D. Meiss and E. Ott, Markov-Tree Model Transport in Area-Preserving Maps, *Physica* **20***D* (1986) 387-402.

[7] I. Dana, N. W. Murray, and I. C. Percival, Resonances and Diffusion in Periodic Hamiltonian Maps, *Phys. Rev. Lett.* **62** (1989) 233-236.

[8] J. M. Greene, R. S. MacKay and J. Stark, Boundary Circles for Area-Preserving Maps, *Physica* **21***D* (1986) 267-295.

[9] B. V. Chirikov, Research Concerning the Theory of Non-linear Response and Stochasticity, Siberian Sec. USSR Acad. Sci. Report 267, CERN trans. 71-40 (1969), and references therein.

S. Aubry, The New Concept of Transition by Breaking of Analyticity in a Crystallographic Model, in *Solitons and Condensed Matter Physics*, A. R. Bishop and T. Schneider, eds. (Springer-Verlag, New York, 1978) 264-278.

I. C. Percival, Variational Principles for Invariant Tori and Cantori, in *Nonlinear Dynamics and the Beam-Beam Interaction*, M. Month and J. C. Herrera, eds., *AIP Conf. Proc.* **57** (1979) 302-310.

[10] I. C. Percival and F. Vivaldi, A Linear Code for the Sawtooth and Cat Maps, *Physica* **27***D* (1987) 373-386.

[11] N. Bird and F. Vivaldi, Periodic Orbits of the Sawtooth Maps, *Physica* **30***D* (1988) 164-176.

[12] Q. Chen and J. D. Meiss, Flux, Resonances and the Devil's Staircase for the Sawtooth Map, *Nonlinearity* **2** (1989) 347-356.

[13] J. R. Cary and J. D. Meiss, Rigorously Diffusive Deterministic Map, *Phys. Rev. A* **24** (1981) 2664-2668.

I. Dana, Hamiltonian Transport on Unstable Periodic Orbits, *Physica D* (1989), in press.

[14] S. Aubry, Exact Models with a Complete Devil's Staircase, *J. Phys. C* **16** (1983) 2497-2508.

[15] A. Katok, Periodic and Quasiperiodic Orbits for Twist Maps, in *Dynamical Systems and Chaos*, L. Garrido, ed., Springer Lect. Notes in Phys. **179** (1983) 47-65.

[16] W. Li and P. Bak, Fractal Dimension of Cantori, *Phys. Rev. Lett.* **57** (1986) 655-658.

R. S. MacKay, Hyperbolic Cantori have Dimension Zero, *J. Phys. A.* **20** (1987) L559-561.

[17] Q. Chen, Area as a Devil's Staircase in Twist Maps, *Phys. Lett.* **123A** (1987) 444-450.

[18] G. H. Hardy and E. M. Wright, *An Introduction to the Theory of Numbers*, (Oxford Univ. Press, Oxford, 1979).

[19] I. Dana and S. Fishman, Diffusion in the Standard Map, *Physica* **17***D* (1985) 63-74.

[20] J. D. Meiss, Class Renormalization: Islands around Islands, *Phys. Rev. A* **34** (1986) 2375-2383.

[21] L. P. Kadanoff and C. Tang, Escape from Strange Repellers, *Proc. Natl. Acad. Sci. USA* **81** (1984) 1276-1279.

[22] T. Bohr and D. Rand, The Entropy Function for Characteristic Exponents, *Physica* **25***D* (1987) 387-398.

Figure Captions

1 Schematic illustration of some points on a (minimizing) hyperbolic ordered periodic orbit (filled circles) and its "minimax" counterpart (open circles) in phase space.

2 Universal form of the turnstile in the principal gap of a sawtooth-map cantorus.

3 Principal island of a sawtooth-map resonance (parallelogram $LERF$). The shaded regions correspond to the upper and lower turnstiles.

4 a) Resonances of the sawtooth map for $K = 0.1$ up to period 10. b) Five resonances of the standard map at $K = 1.972$. Note that away from the central gap, around $x = 0$, the resonances have a rectangular shape similar to the sawtooth map.

5 The area devil's staircase function in the sawtooth map at $K = 0.3$. Only half the staircase is plotted. The other half can be obtained by the reflection symmetry: $A(1 - \nu) = 1 - A(\nu)$.

6 Principal island of a resonance when $\lambda^n > 3$, with its generalized turnstiles (shaded regions). The darker shading indicates outgoing flux.

7 Overlaps, $\mathcal{F}(m/n \to m'/n')$ and $\mathcal{F}(m'/n' \to m/n)$ (shaded regions), of the generalized turnstiles of two resonances $(m,\ n)$ and $(m',\ n')$ when $m/n > m'/n'$.

8 Critical value $K_c(n)$ for the onset of turnstile overlap of the $(0,\ 1)$ and $(1,\ n)$ resonances as a function of n.

9 Illustration of $\mathcal{L}$-$\mathcal{R}$ coding for the $(1,\ 2)$ resonance.

10 Construction of the horseshoe for trapped orbits. Notation for the homoclinic points is the same as for Fig. 6. a) For $\lambda > 3$, the trapped regions are contained in the strips $\mathcal{V}_1$, $\mathcal{V}_2$, while region $\mathcal{M}$ is the union of the outgoing halves of the turnstiles. b) Upon iteration by T^n, $\mathcal{V}_1$ becomes $\mathcal{H}_1$ and $\mathcal{V}_2$ becomes $\mathcal{H}_2$. c) Regions $\mathcal{V}_1$, $\mathcal{V}_2$ and $\mathcal{M}$ for $2 < \lambda < 3$.

11 Trapped periodic orbits, computed using the $\mathcal{L}$-$\mathcal{R}$ code: a) $\lambda = 3.2$, maximum period is 8; b) $\lambda = 2.4$, maximum period is 12; c) $\lambda = 1.8$, maximum period is 12; d) $\lambda = 1.2$, maximum period is 12.

12 Trapped rotational periodic orbit with frequency $1/11$ as λ varies from one to three.

13 Rotational orbit of even period q (under the map T^n) inside the principal island of a resonance but outside the turnstiles (dashed regions).

14 Trapped rotational periodic orbit with frequency $3/10$. The orbit is born from the minimax point (the origin) with two of its points (those on the S-shaped curve) on the wrong side of the discontinuity line. These points cross to the proper side at a larger value of λ.

15 Set of trapped rotational periodic orbits for all frequencies up to a a maximum period of thirty. Here, $\lambda = 1.2$, as in Fig. 11d.

16 Number of periodic points trapped in a resonance as a function of period q at $\lambda = 2.4$. The number is shown on a logarithmic axis with a base $h = 1.859$, which is the exponential of the entropy. For periods 18 and 19, $N(q)$ deviates from the exponential behavior, due to numerical error in checking the existence condition (2).

17 a) Survival probability from a Monte Carlo experiment with 10^6 initial conditions. b) Average escape rate from (58).

18 Escape rate as a function of the Lyapunov multiplier. The smooth line is the Markov rate, (56). The dark line is the Lyapunov rate, (57), which is determined numerically within a 2% relative error. The triangles are numerical rates, (58).

19 Escape rate as a function of the residue. The straight line is the Markov rate, and the triangles are numerical rates. The smooth curve is the least-square fit to a power law.

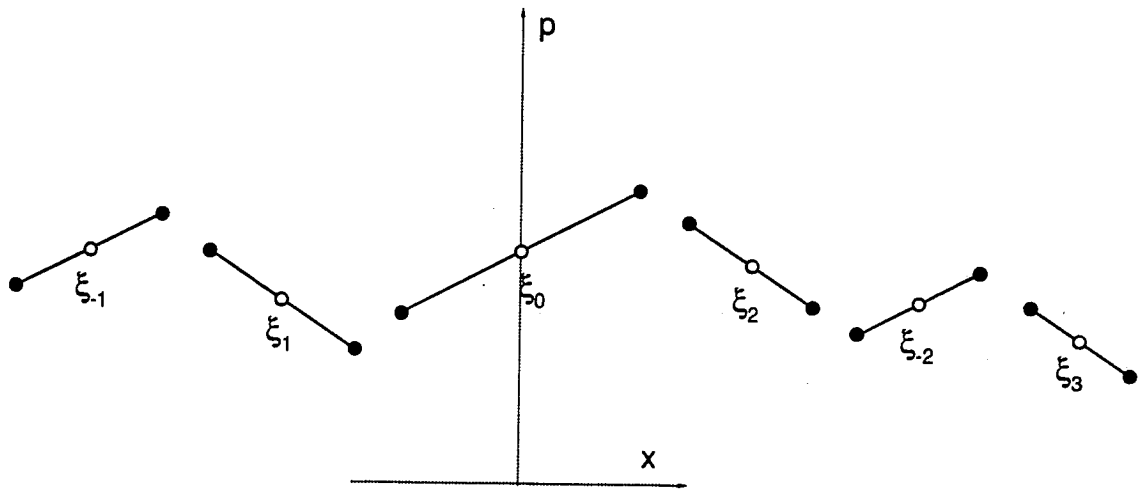

Figure 1

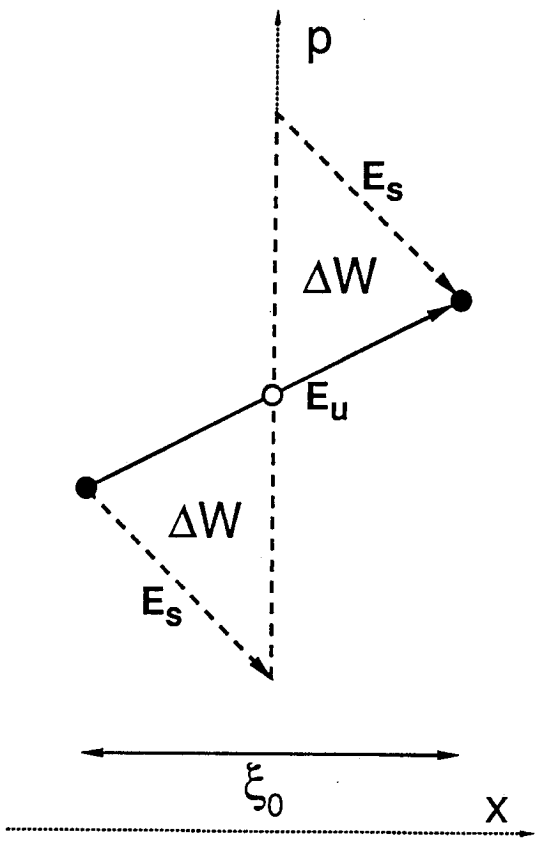

Figure 2

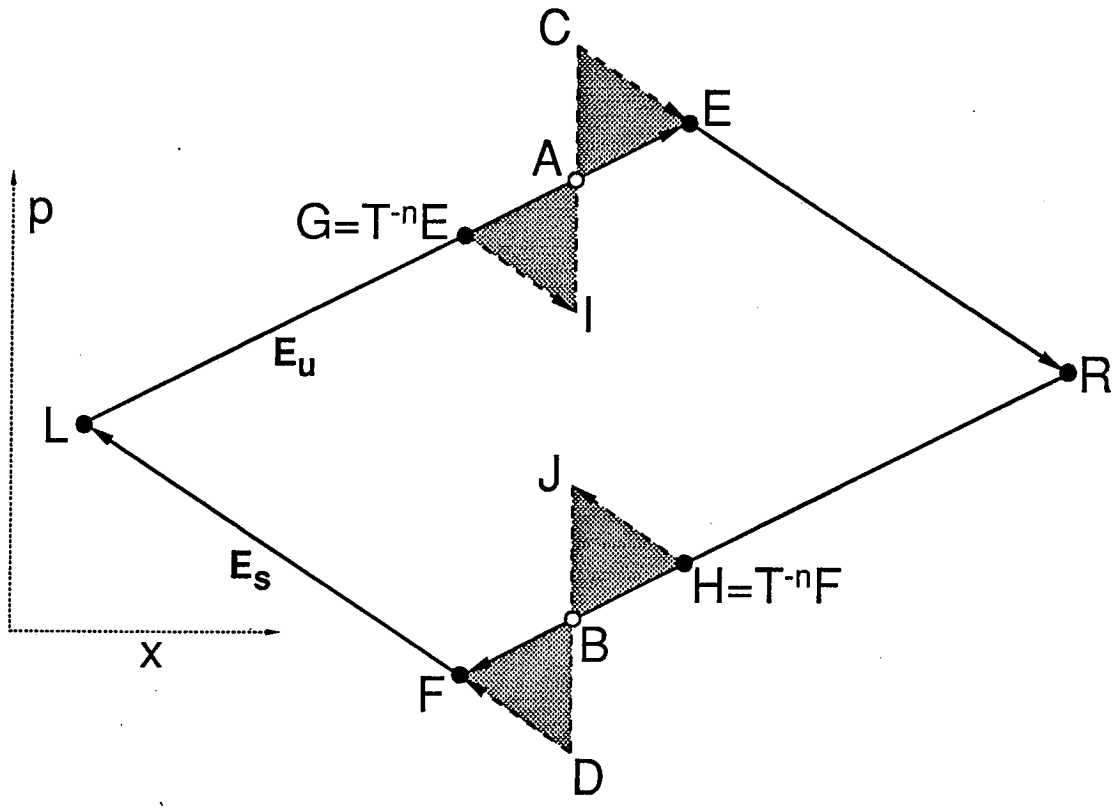

Figure 3

Figure 4a

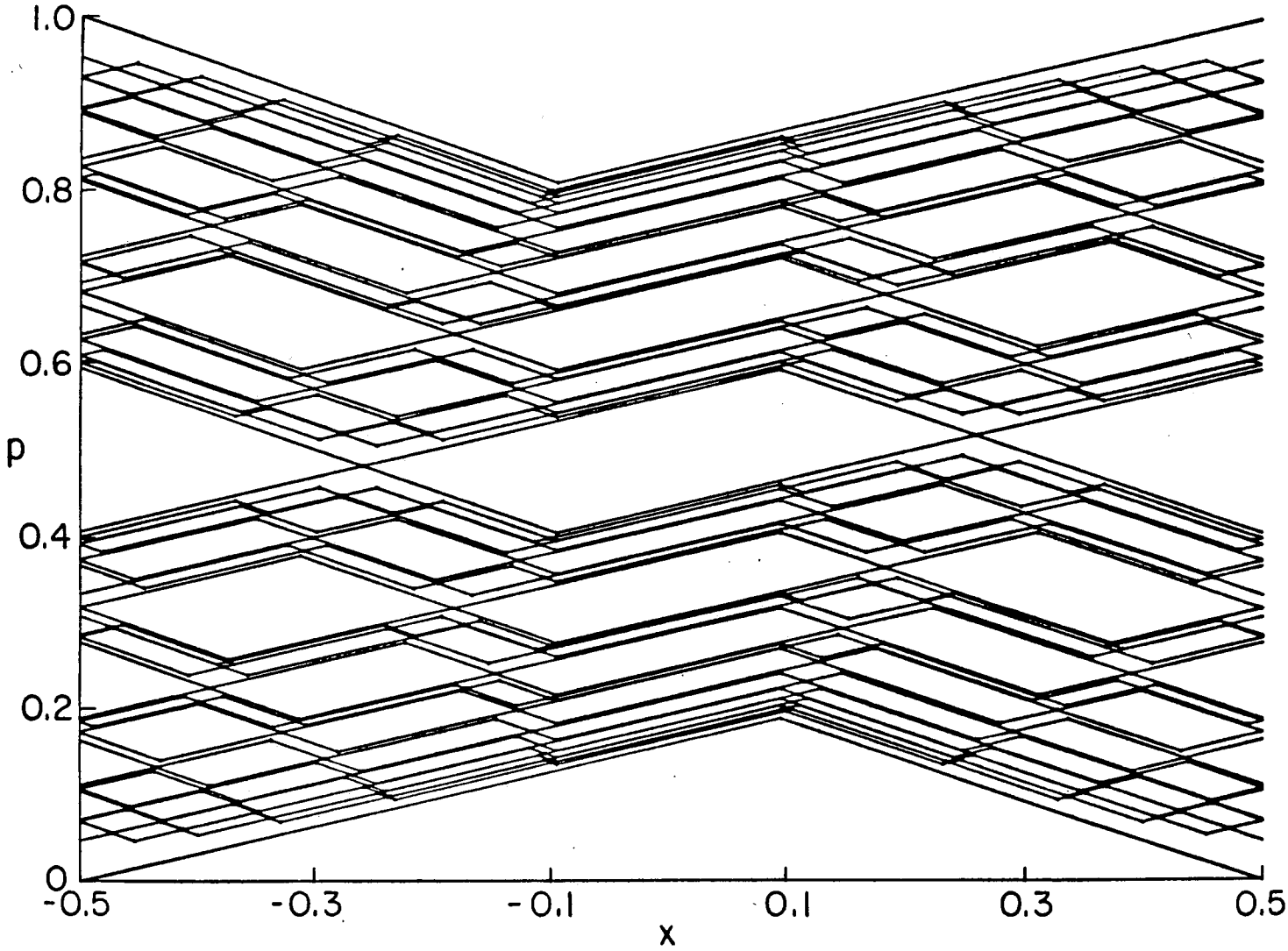

Figure 4b

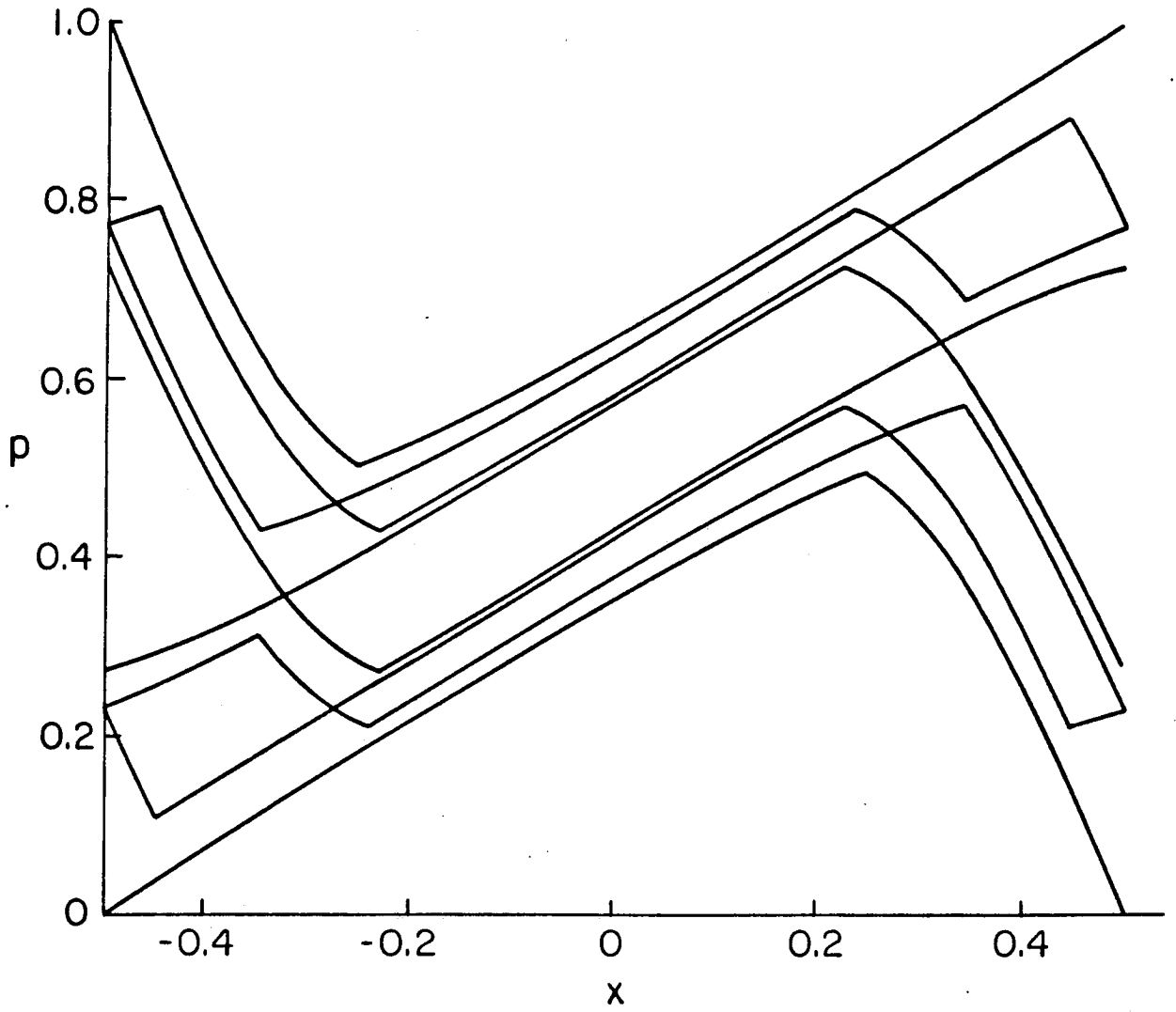

Figure 5

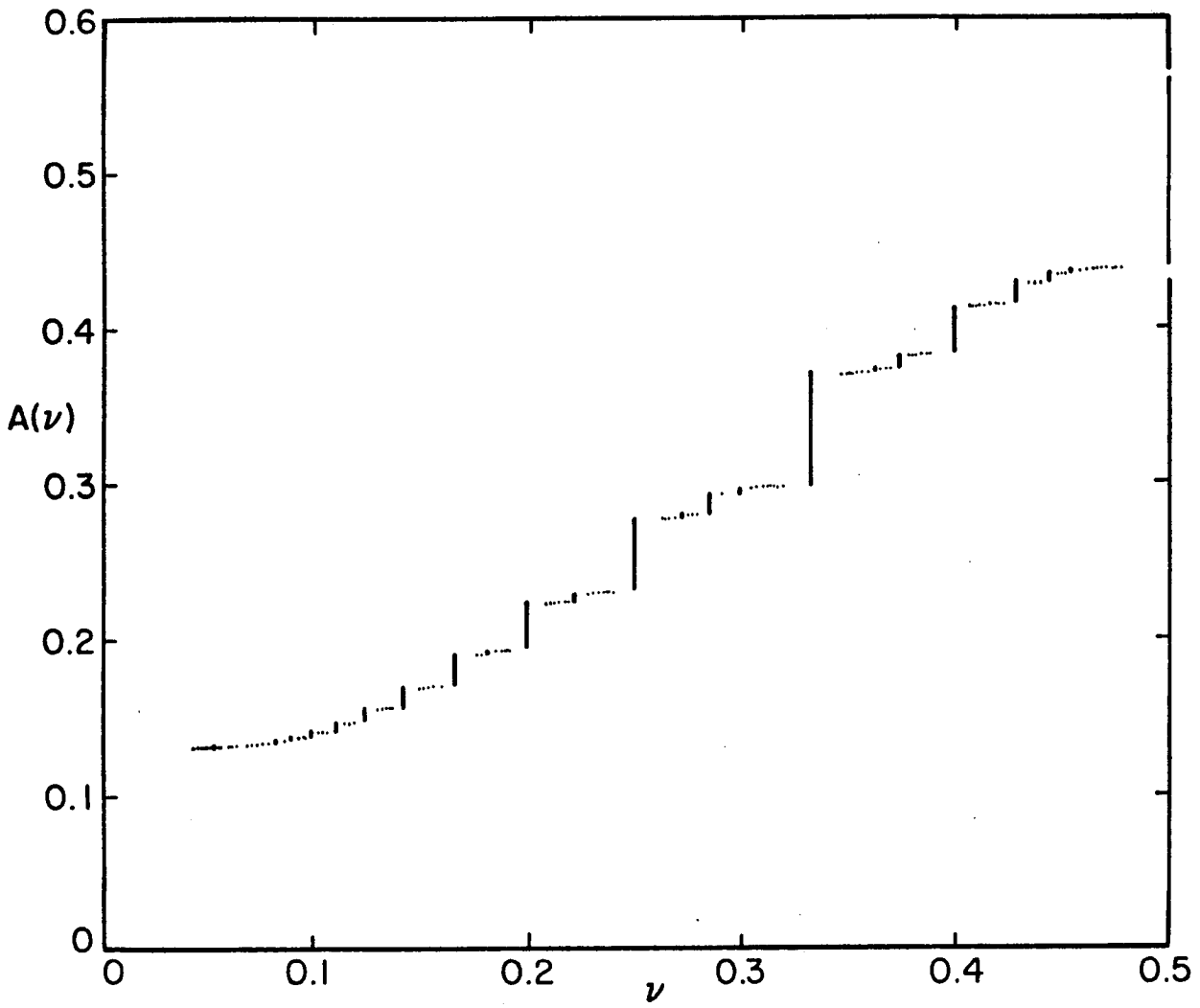

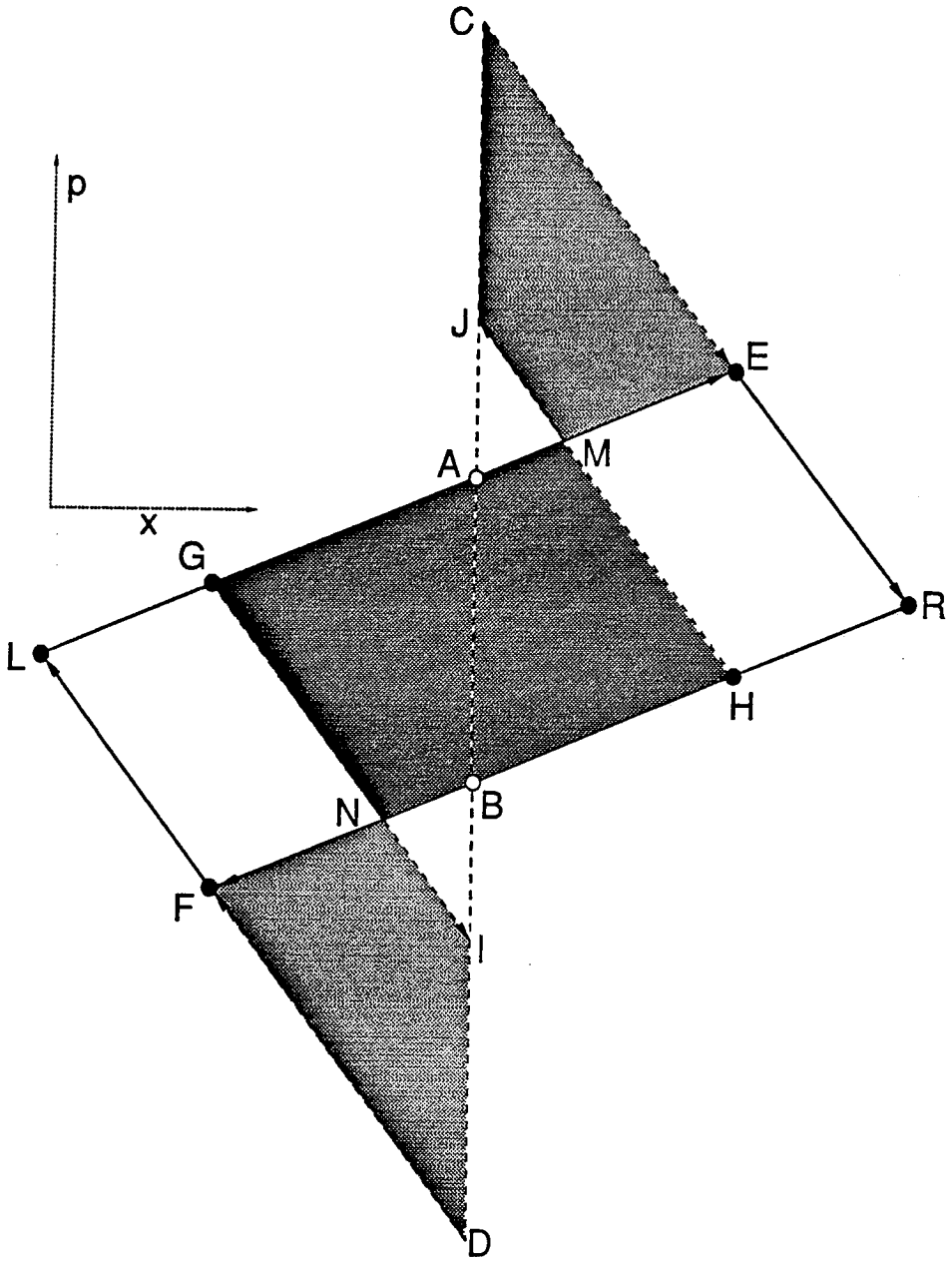

Figure 6

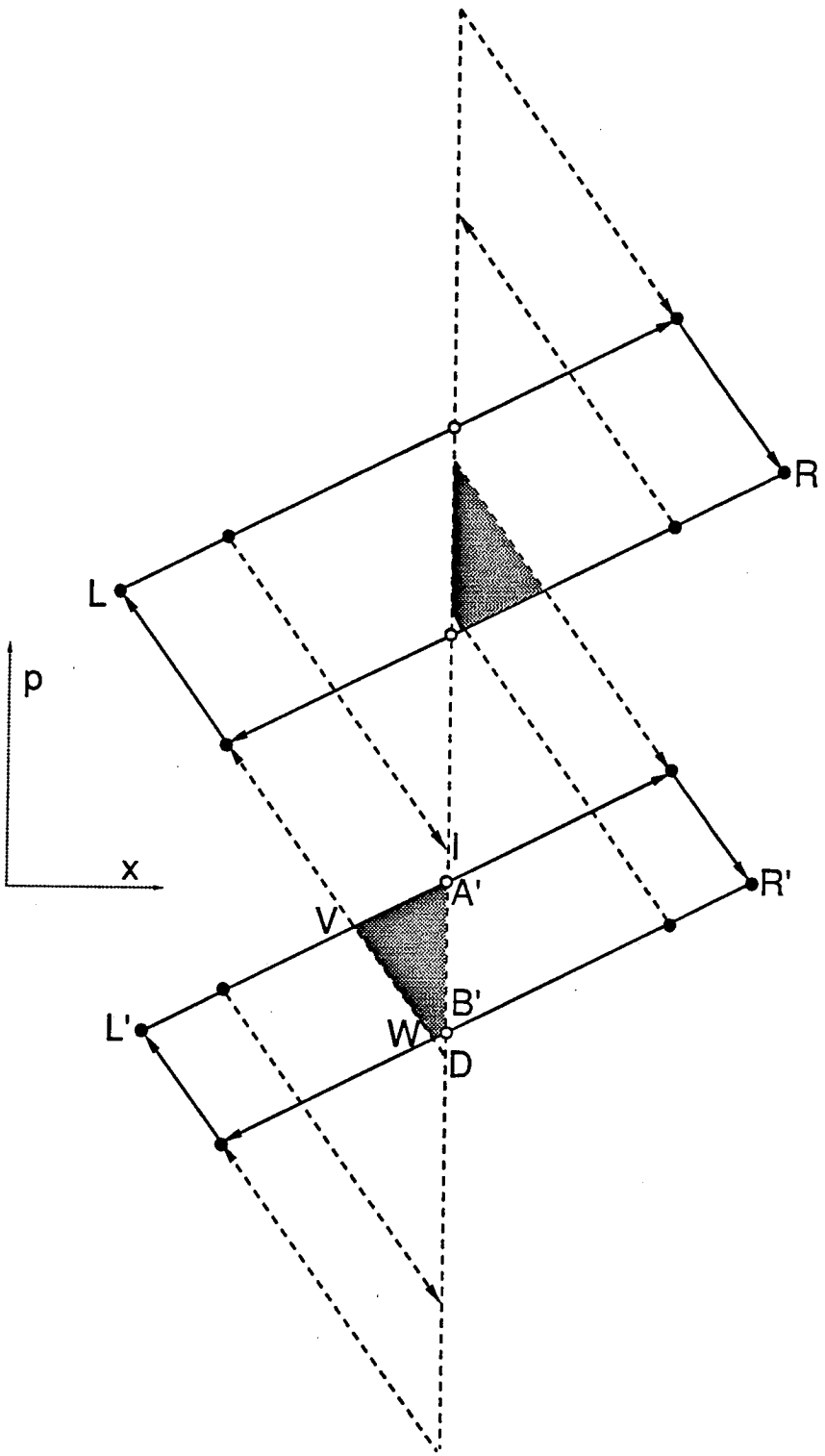

Figure 7

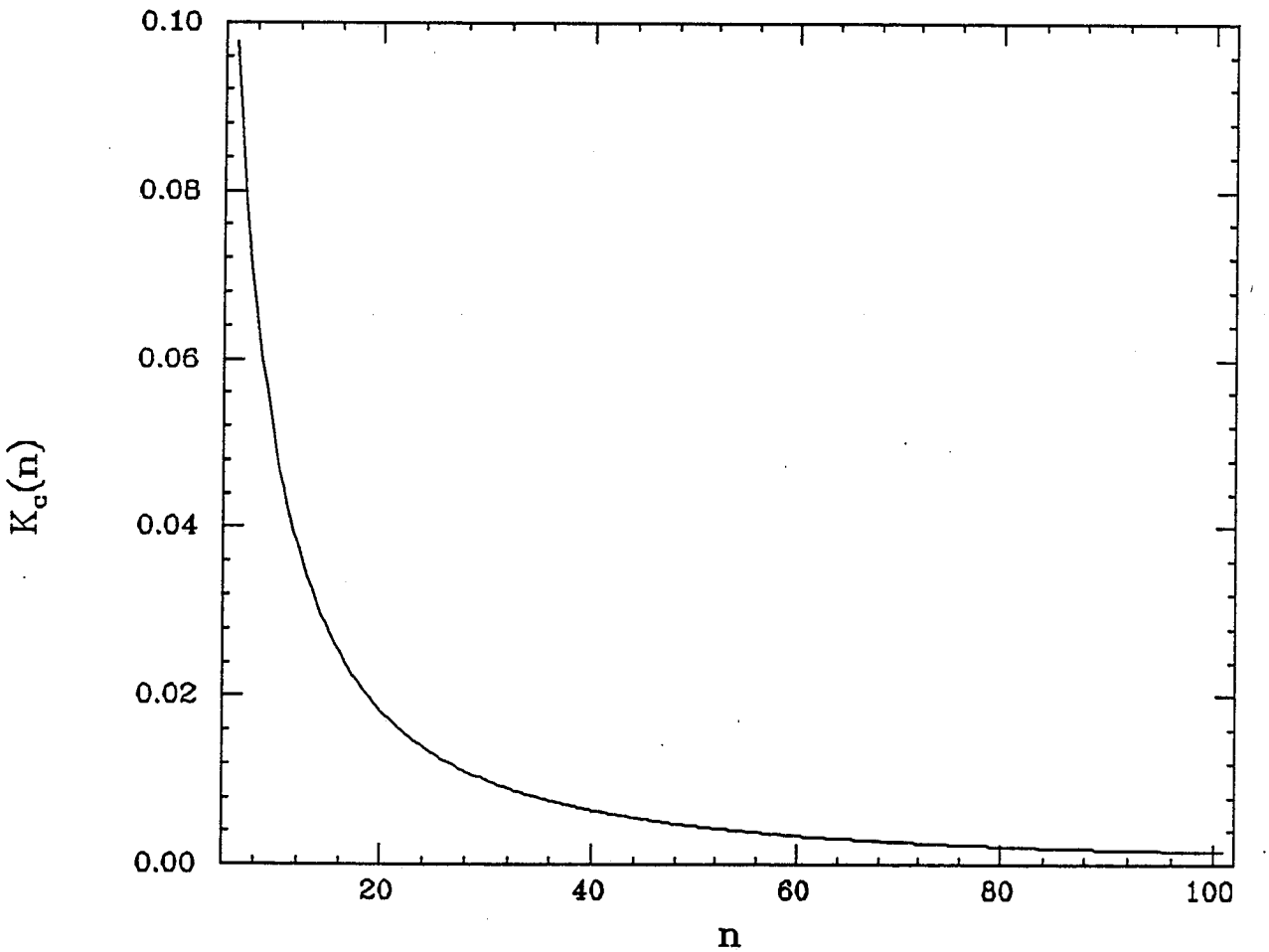

Figure 8

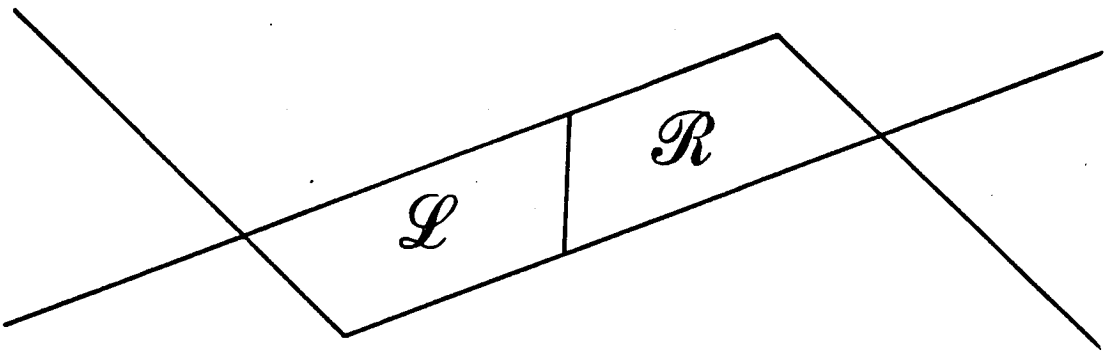

Figure 9

Figure 10a

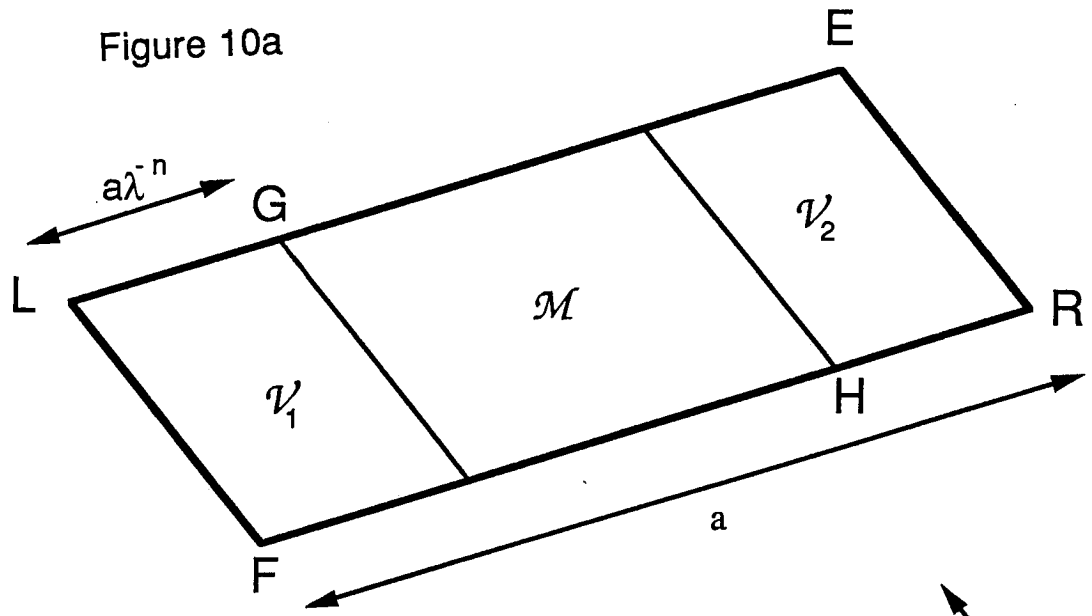

Figure 10b

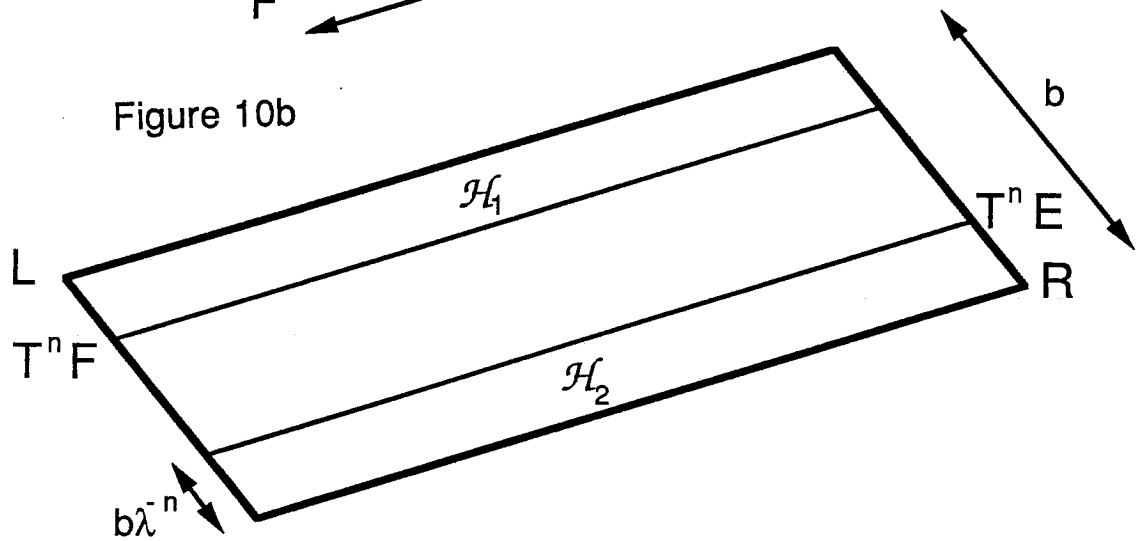

Figure 10c

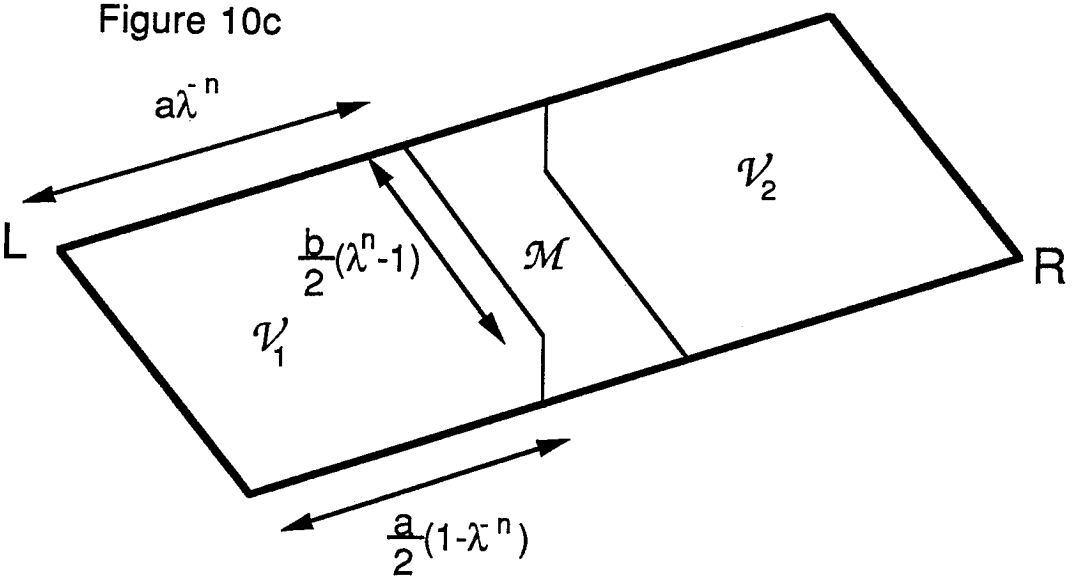

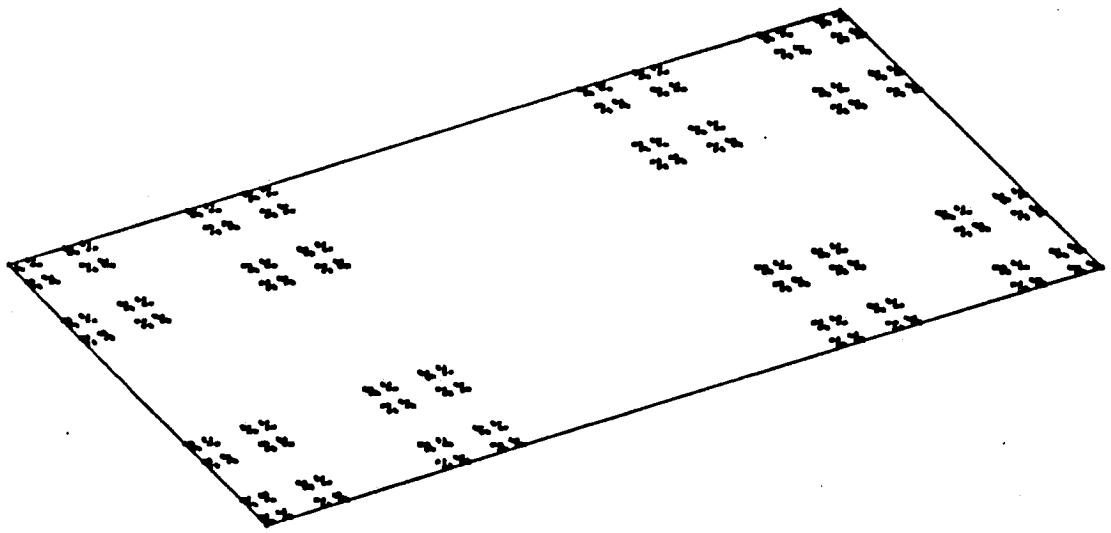

Figure 11a

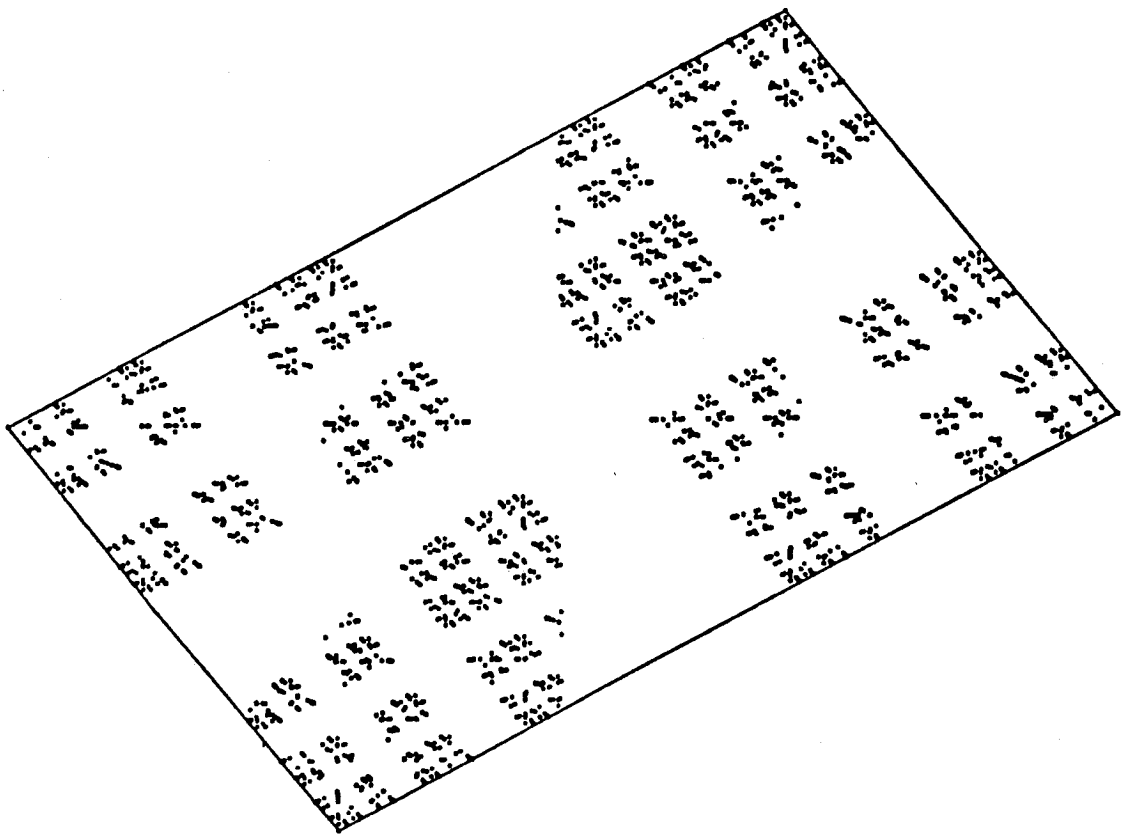

Figure 11b

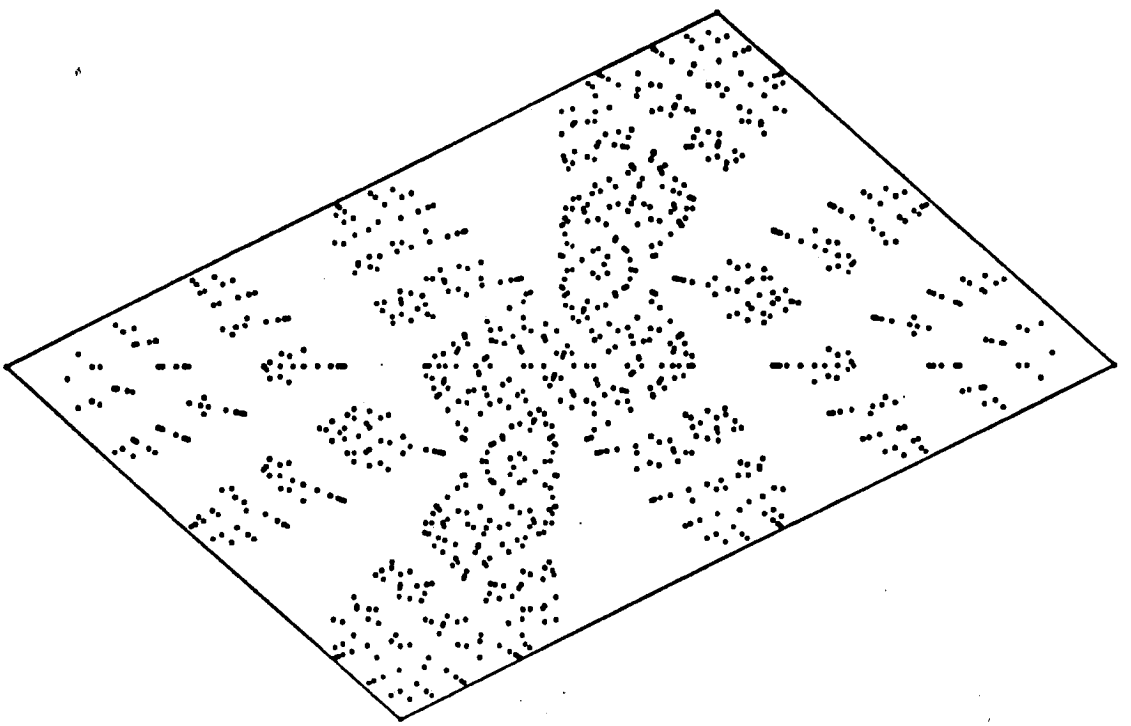

Figure 11c

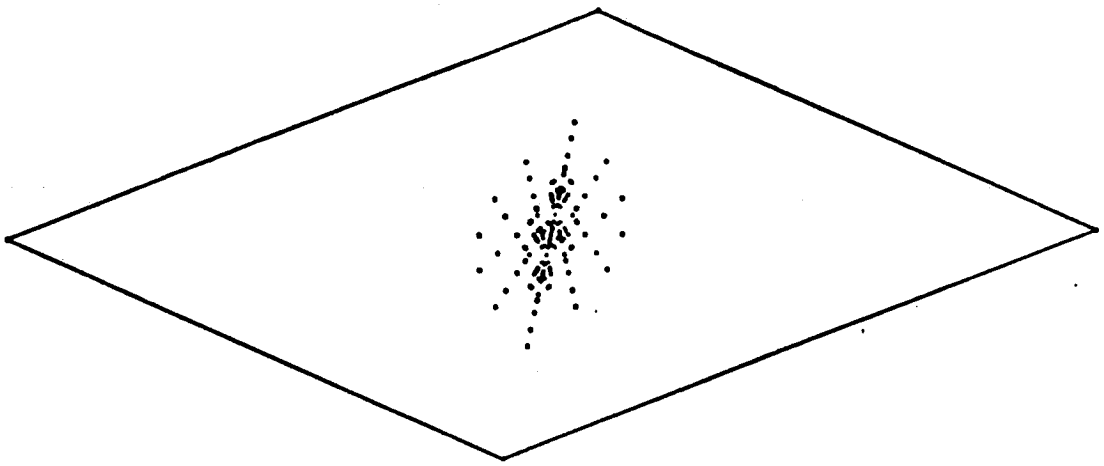

Figure 11d

Figure 12

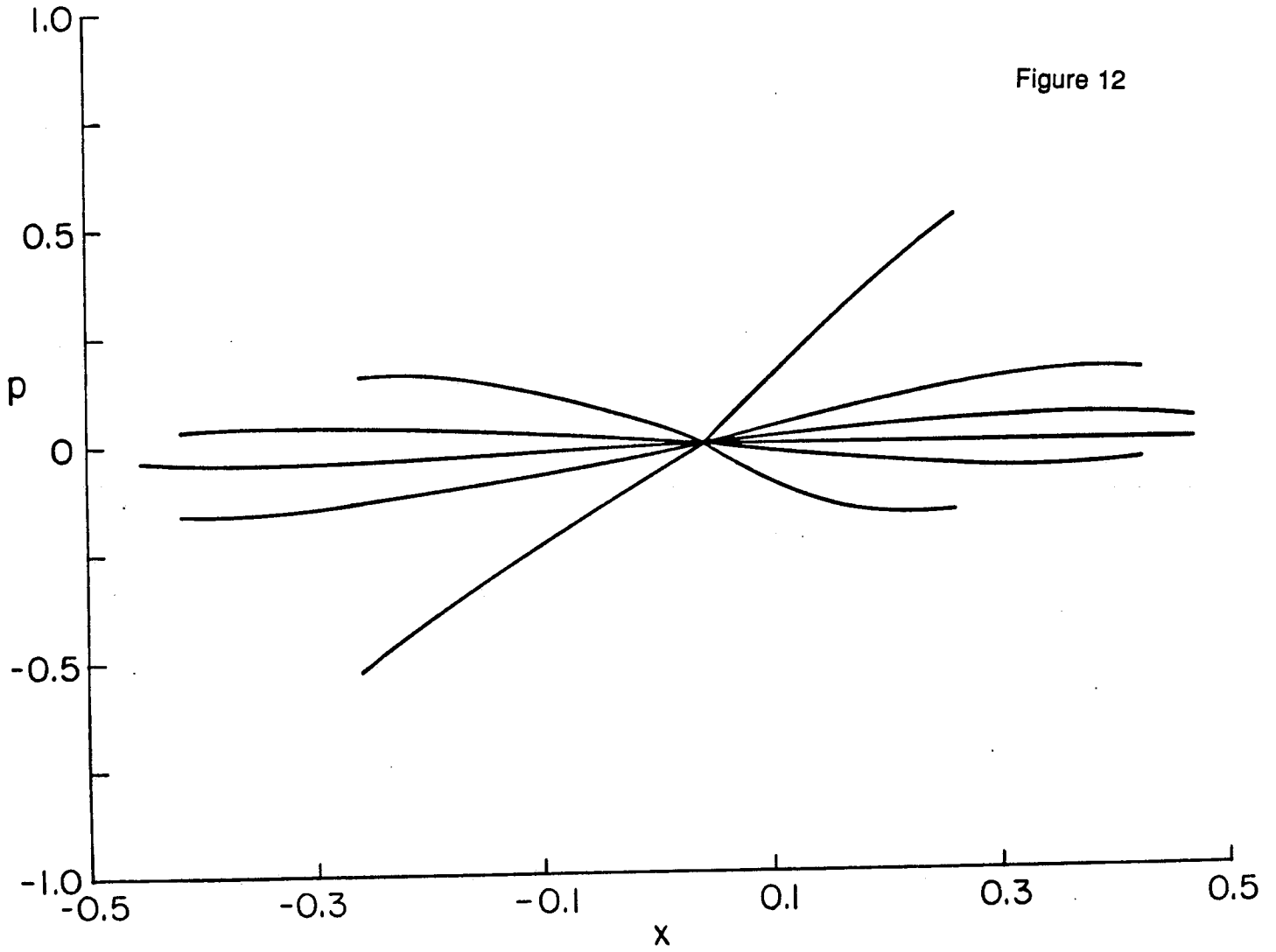

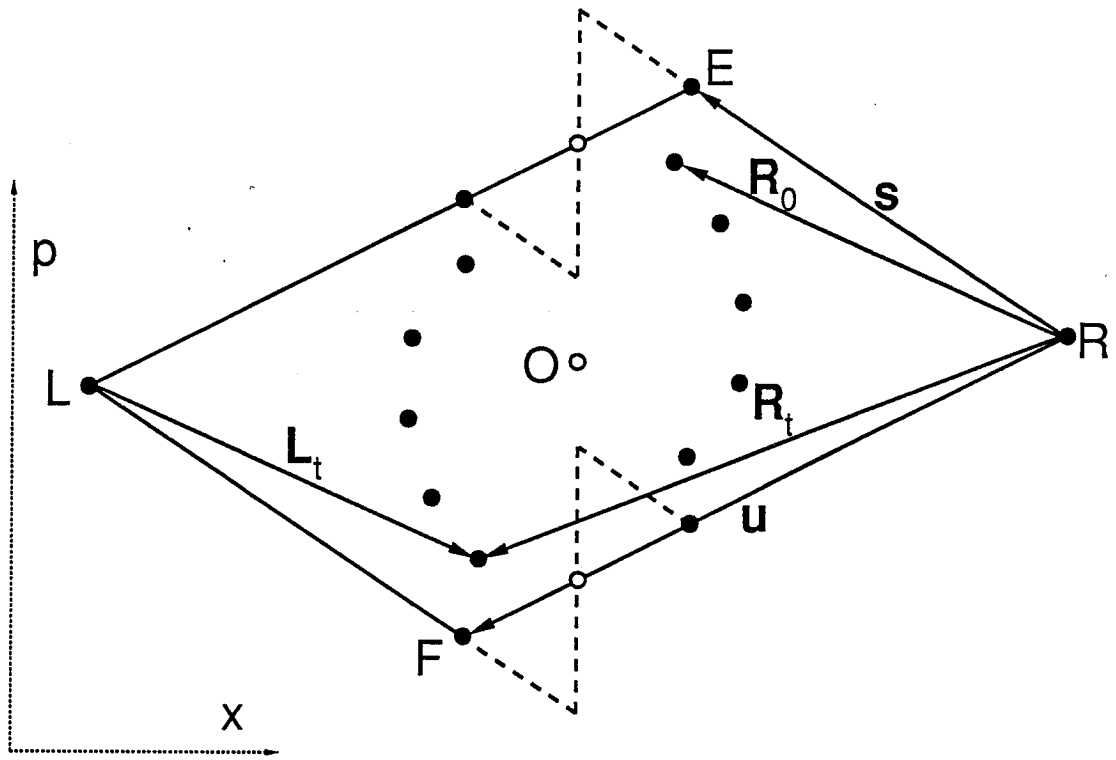

Figure 13

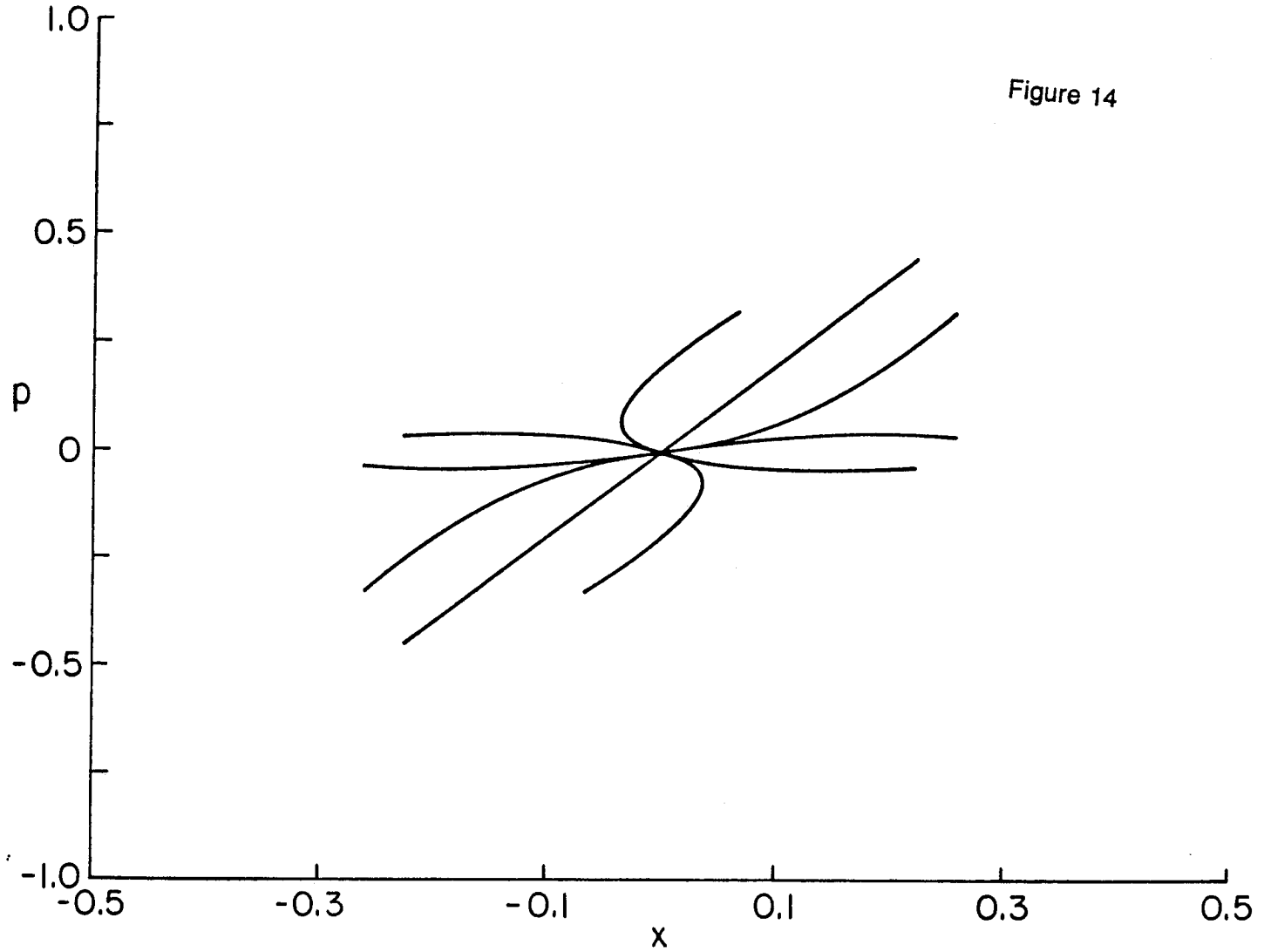

Figure 14

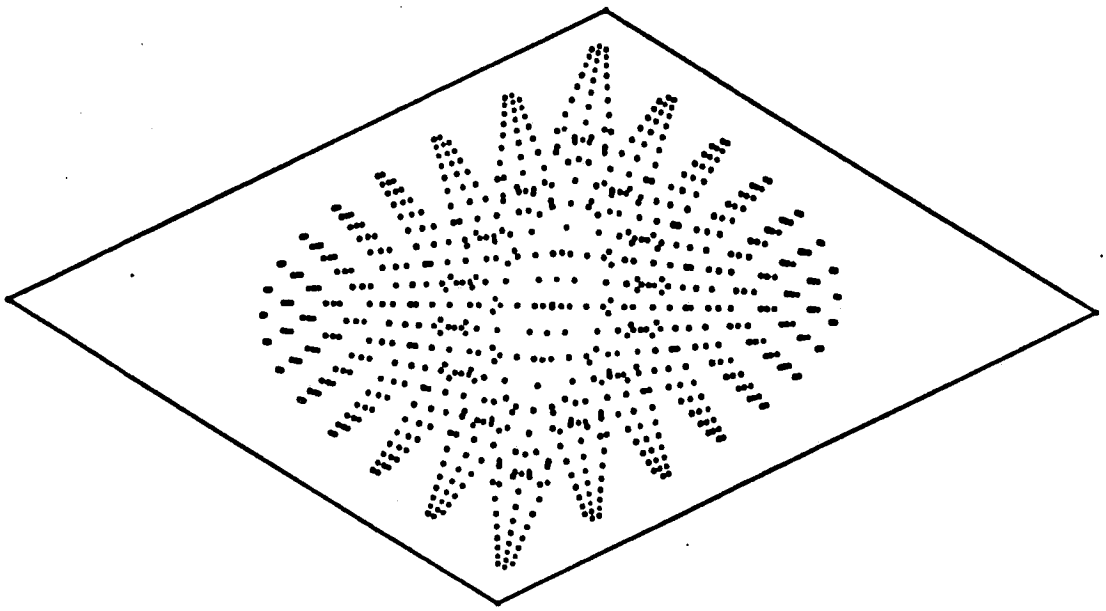

Figure 15

Figure 16

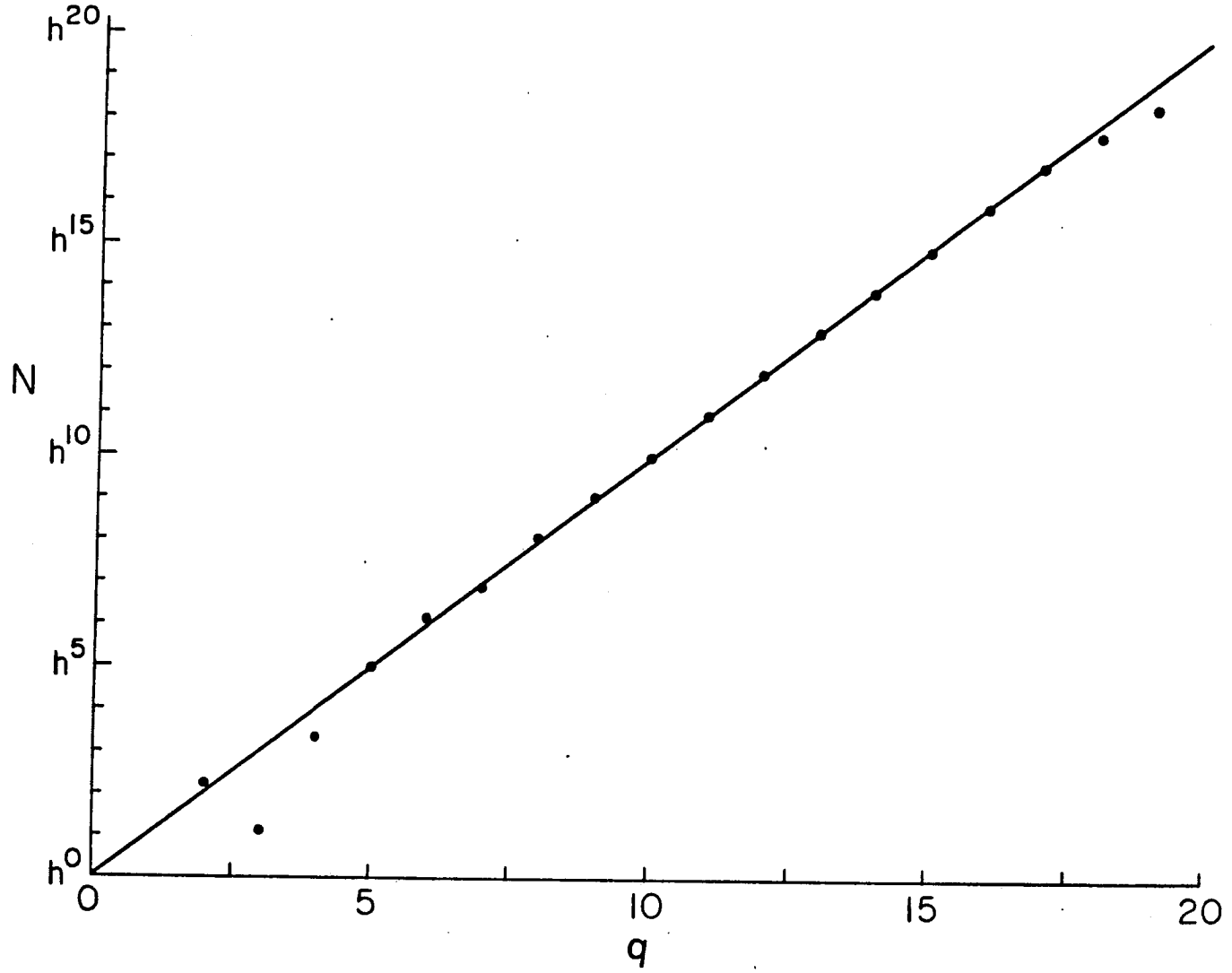

Figure 17a

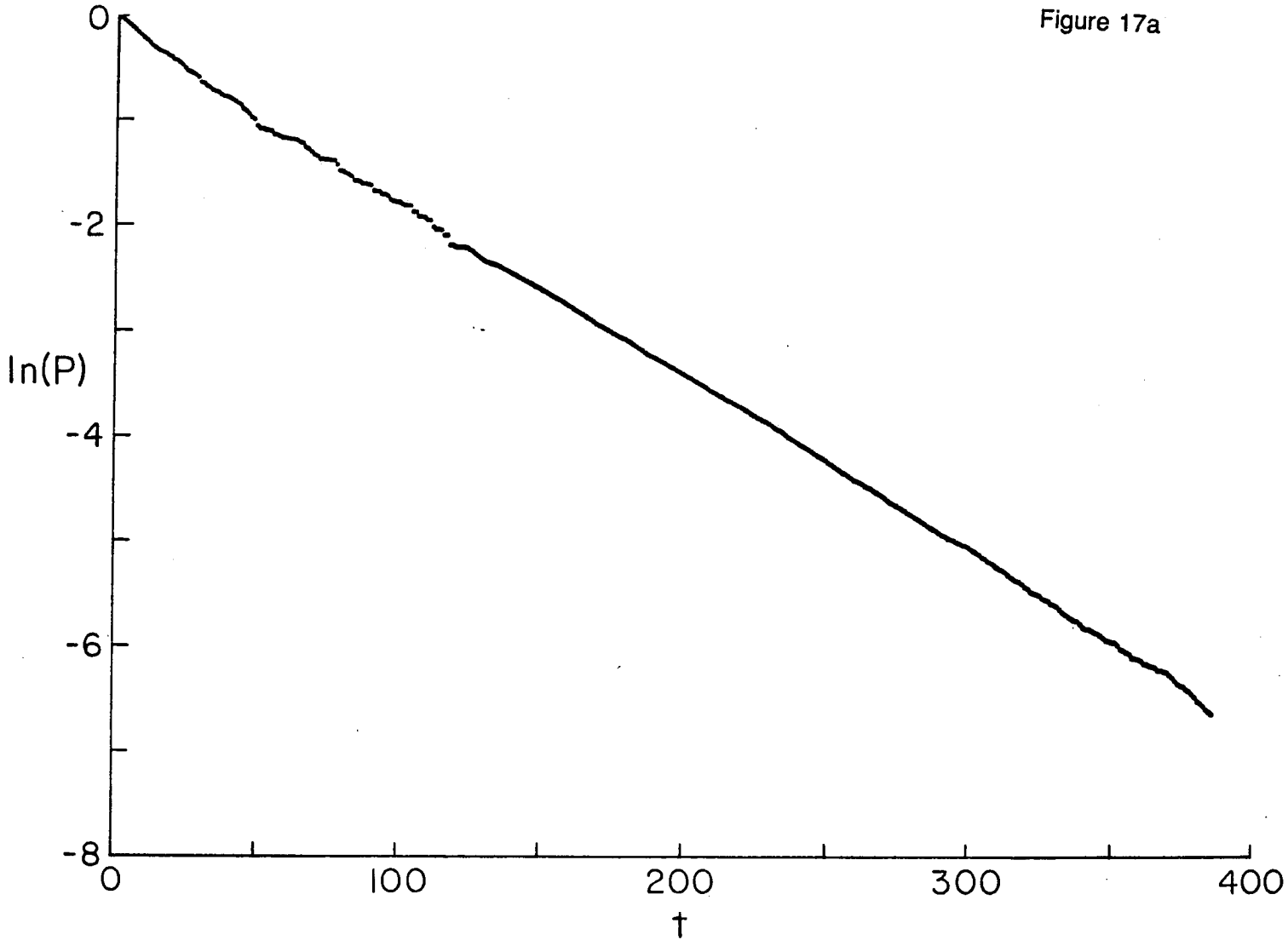

Figure 17b

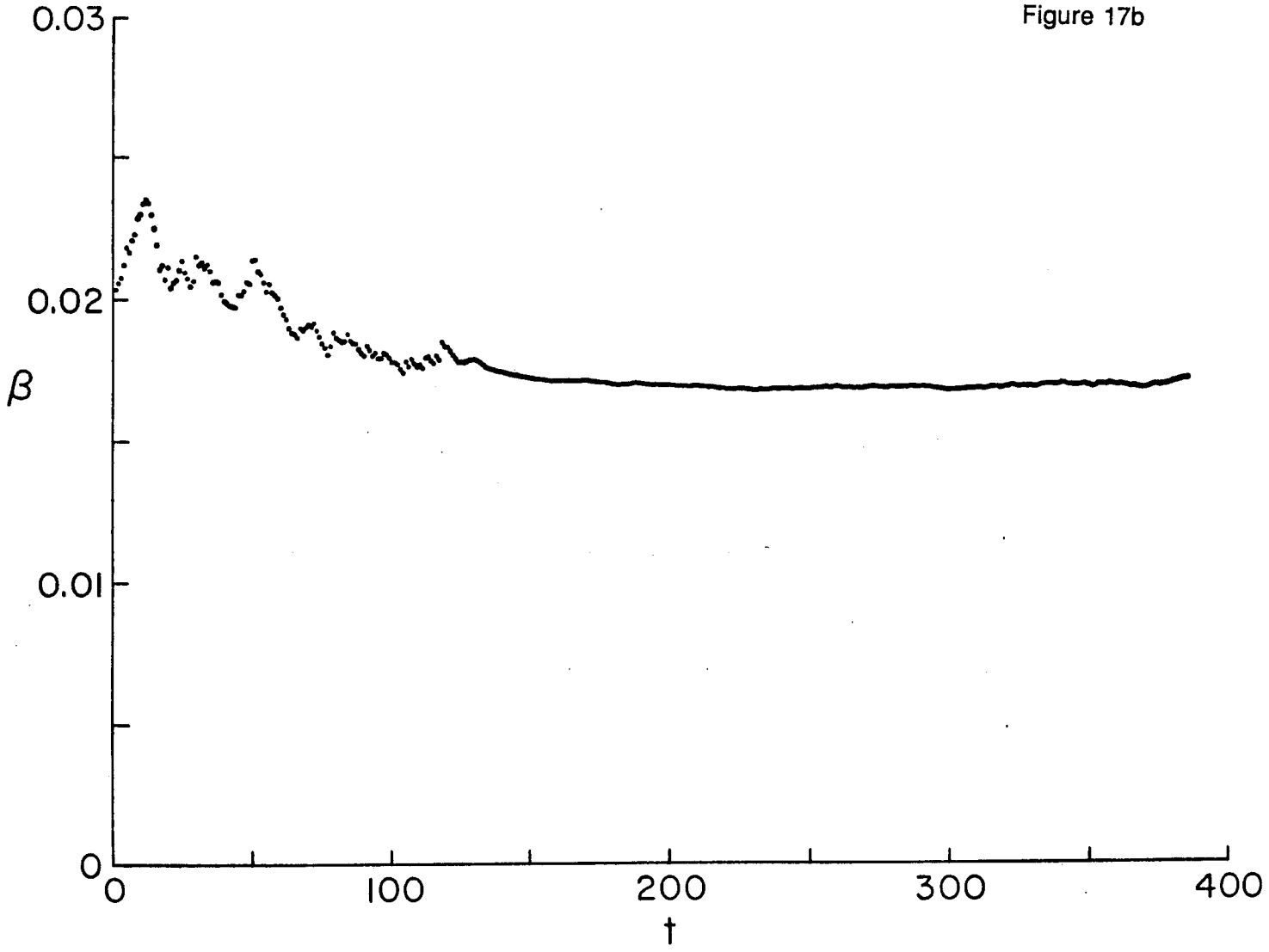

Figure 18

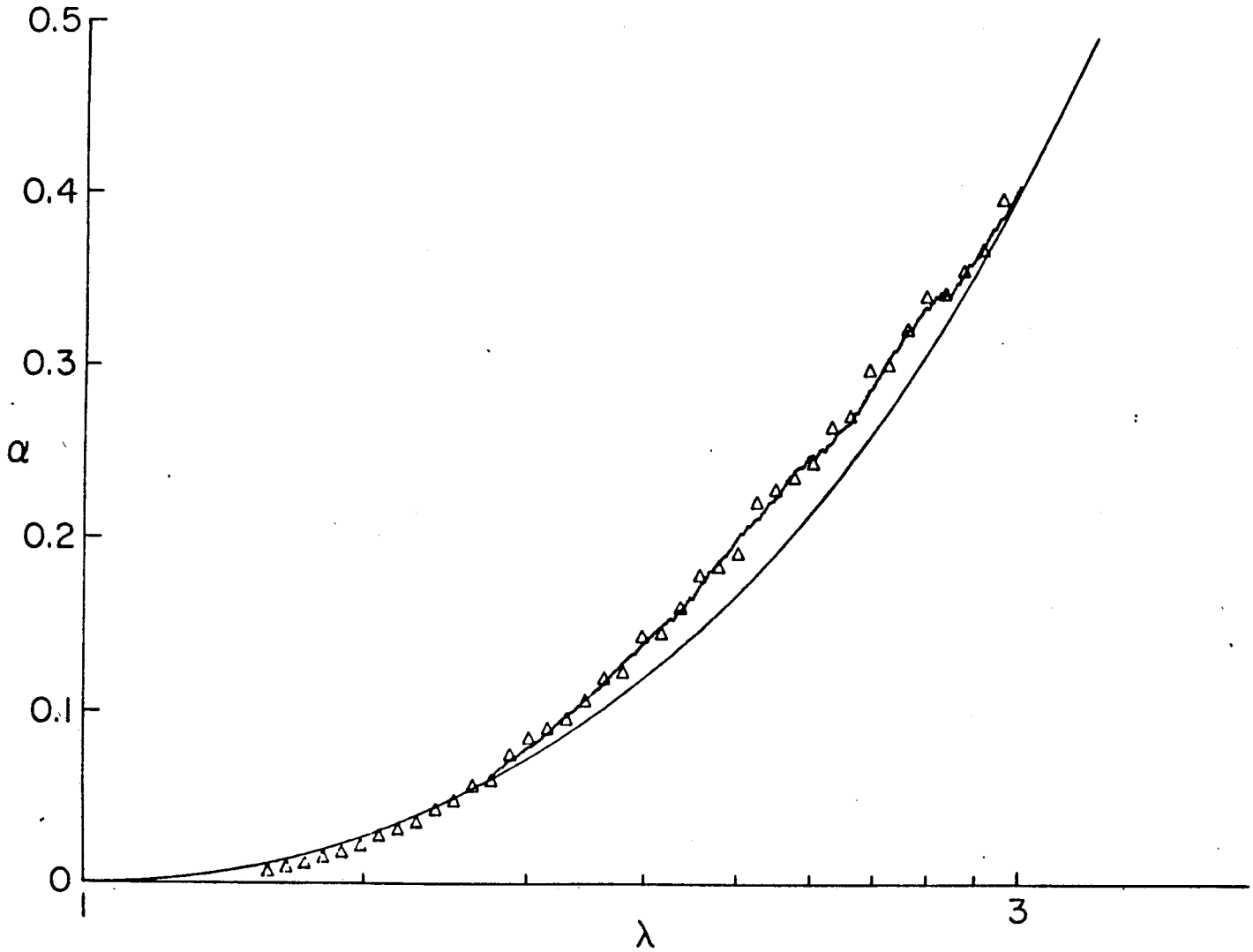

Figure 19